Supporting Information

Gas Phase Identification of the Elusive N-Hydroxyoxaziridine ($c\text{-}H_2CON(OH)$) – A Chiral Molecule

Santosh K. Singh[a], Tang-Yu Tsai[b], Bing-Jian Sun[b], Agnes H.H. Chang*[b], Alexander M. Mebel[c]
Ralf I. Kaiser*[a]

[a]*Department of Chemistry, University of Hawaii, 2545 McCarthy Mall, 96822 HI, USA*
W. M. Keck Research Laboratory in Astrochemistry, University of Hawaii, 96822 HI, USA

[b]*Department of Chemistry, National Dong Hwa University, Shoufeng, Hualien 974, Taiwan*

[c]*Department of Chemistry and Biochemistry, Florida International University, Miami, Florida 33199, USA*

*Corresponding authors. E-mail: ralfk@hawaii.edu, hhchang@gms.ndhu.edu.tw

METHODS

Experimental

Experiments were conducted in an ultrahigh vacuum chamber evacuated to a base pressure of a few 10^{-11} torr using turbo molecular pumps backed by dry scroll pumps.[1-2] To prepare each ice mixture, gases of methane (CH_4; 99.95% Sigma Aldrich) and nitrogen dioxide (NO_2; 99.95% Sigma Aldrich) were premixed and deposited at 5×10^{-8} torr via glass capillary onto a silver substrate which is mounted on a cold finger made from oxygen free high conductivity copper. The temperature of the cold finger was maintained at 4.9 ± 0.2 K using closed cycle helium refrigerator (Sumitomo Heavy Industries, RDK-415E) during deposition of the gases. The ice mixtures of ^{13}C-methane ($^{13}CH_4$) and nitrogen dioxide (NO_2) as well as deuterated-methane (CD_4) and NO_2 were prepared in the similar way. The thickness of each ice of 550±50 nm was determined *in situ* via laser interferometry (SI). The ratio of methane to nitrogen dioxide in the ice mixture was found to be 1.2±0.4:1 by using the integrated infrared absorption coefficients of 9.71×10^{-18} (1297 cm^{-1}) and 6.24×10^{-18} cm molecule^{-1} (1613 cm^{-1}), respectively.[3-4] The infrared spectra of the ice mixtures were collected in the 6000-600 cm^{-1} region using a Fourier Transform Infrared Spectrometer (Nicolet 6700) operated at a resolution of 4 cm^{-1}. Then, each ice mixture was exposed to 5 keV energetic electrons at an angle of 70º to the normal of the substrate at an electron current of 20 ± 2 nA for 15 min. IR spectra of the ices were measured *in situ* during irradiation to monitor the changes induced by ionizing radiation. Using Monte Carlo simulations via CASINO 2.42 software,[5] the average penetration depth of the electrons in the ice mixture was found to be 289±30 nm and the average energy deposited was calculated to be 1.2±0.2 eV per molecule. Hereafter, ices were annealed at a rate of 1 K min^{-1}, and molecules subliming from the substrate were ionized and detected using photoionization along with reflectron time-of-flight mass spectrometry (PI-ReTOF-MS). Pulsed VUV light is utilized for the photoionization of the molecules. Three VUV energies at 10.49 eV, 10.20 eV, 9.80 eV, and 9.70 eV were used to differentiate between isomers of oxaziridine. The ions formed are extracted and eventually separated based on their mass-to-charge (m/z) ratio before reaching to microchannel plate (MCP) detector. The MCP detector generates a signal when ions reach to the detector. This signal is amplified using a preamplifier (Ortec 9305) and shaped with a 100 MHz discriminator. The discriminator sends the signal to a computer based multichannel scaler, which records the signal in 4 ns bins triggered at 30 Hz by a pulse delay generator. 3600 sweeps were collected for each mass spectrum per 1 K increase in the temperature during the TPD phase.

Computational

The reactions between carbene (CH_2) and nitrous acid (HONO) proceeding on the triplet and singlet potential energy surfaces (PESs) are investigated. Collision complexes were identified, their mutual conversion and subsequent isomerization of c-H_2CON(OH) (**1**) were characterized. The geometries of these species and transition states were optimized along with the harmonic frequencies by utilizing coupled cluster CCSD/cc-pVTZ calculations.[6-7] This theoretical method could provide accuracy of 1-2 pm for bond lengths and 1-2° for bond angles. In addition, the anharmonic frequencies and the IR spectrum of molecule **1** are predicted. Their CCSD(T)/cc-pVDZ, CCSD(T)/cc-pVTZ, and CCSD(T)/cc-pVQZ energies were computed and extrapolated to complete basis set limits,[8] CCSD(T)/CBS, with CCSD/cc-pVTZ zero-point energy corrections. These energies are expected to be accurate within 4 kJ mol^{-1}.[9] The triplet - singlet minimum energy crossing points (MSX) were located with CPMCSCF[10]/TZVPP method with energy refined via CCSD(T)/CBS. The intrinsic reaction coordinate (IRC) calculations at CCSD/cc-pVTZ//CCSD(T)/CBS level were carried out to probe the entrance of singlet CH_2 + HONO $\rightarrow$ **1, 4, 6** channels**.** Multi-reference CI (MRCI) calculations are also performed on CCSD/cc-pVTZ optimized geometries to assess the multi-reference effects, in which the reference space and molecular orbitals were provided by MCSCF(8,8), 8 active electrons in 8 orbitals. Likewise, MRCI/cc-pVDZ, MRCI/cc-pVTZ, and MRCI/cc-pVQZ results with Davidson corrections were extrapolated to obtain the MRCI/CBS energies with CCSD/cc-pVTZ zero-point energy corrections. MCSCF(8,8) generates reference space of 1764 and 2352 CSFs (configuration state functions), for singlet and triplet surfaces, respectively. As a result, the MRCI/cc-pVQZ correspondingly consists of 75669972, and 129051696 CSFs. The MRCI/CBS and CCSD(T)/CBS energies are expected to be accurate within 4 and 8 kJ mol^{-1}, respectively.[6] The GAUSSIAN 16 program[11] was employed in coupled cluster calculations, and MOLPRO[10] was used for the surface-crossing, MCSCF, and MRCI computations.

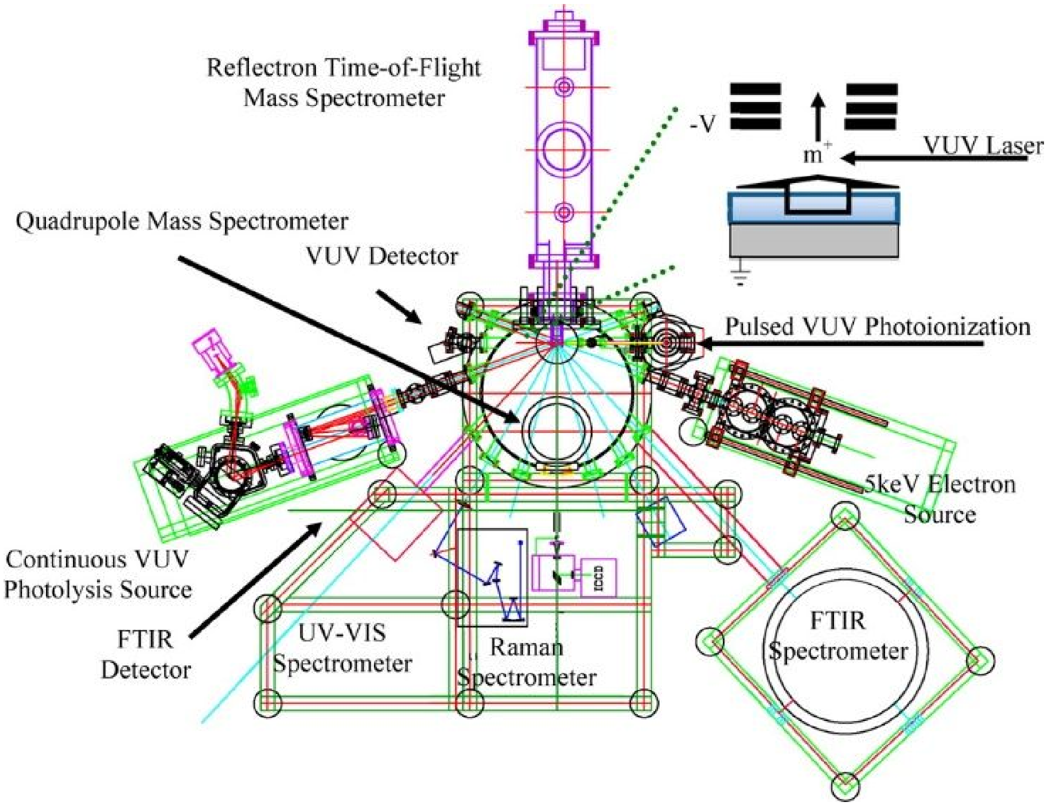

Figure S1. Schematic top view of the ultra-high vacuum chamber including the electron source, analytical instruments (FTIR, UV-VIS, ReTOF), and cryogenic target (point of convergence lines)[1, 12].

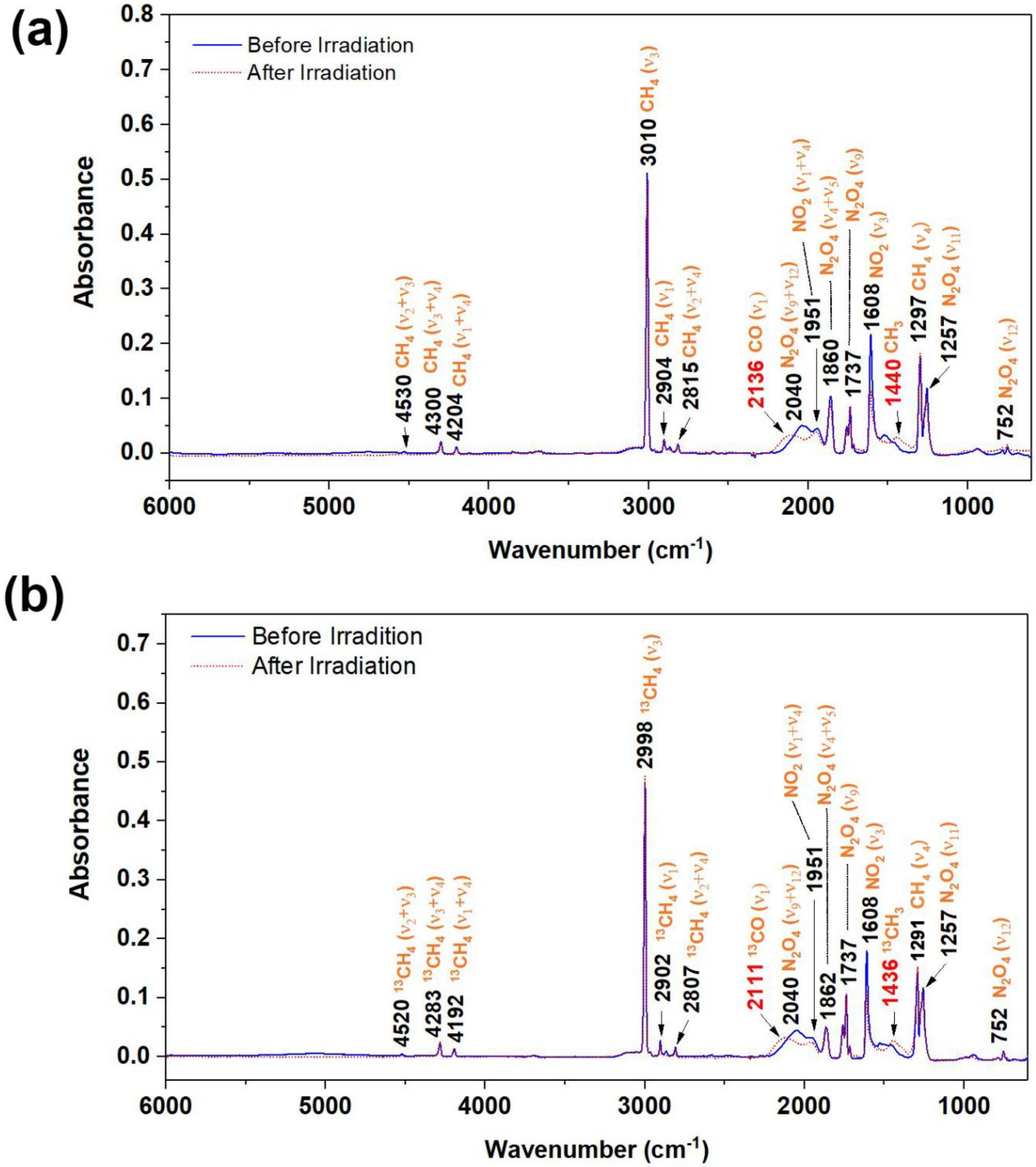

Figure S2. Infrared (IR) spectra of (a) CH_4 + NO_2, (b) $^{13}CH_4$ + NO_2, ice mixtures before and after the irradiation. Detailed assignments of the bands are provided in Table S1 and S2. New bands observed after irradiation are indicated in red color.

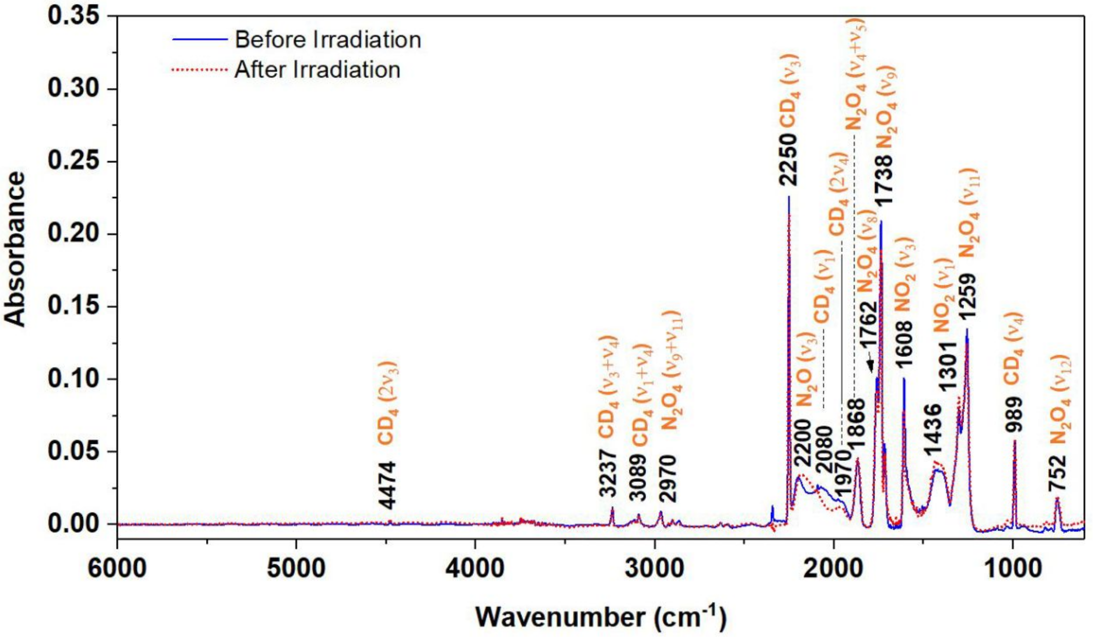

Figure S3. Infrared (IR) spectra of CD_4 + NO_2 ice mixture before and after the irradiation. Detailed assignments of the bands are provided in Table S3. New bands observed after irradiation are indicated in red color.

The FTIR spectrum measured after the irradiation revealed new bands at 2136, 1694, and 1440 cm-1 (Supplementary Fig. S2a, Table S1). Absorptions at 2136, 1694, and 1440 cm-1 can be associated with vibrations of carbon monoxide (CO), nitrous acid (HONO) and methyl group (-CH3) respectively.[13-14] The peaks corresponding to N-hydroxyoxaziridine (c-H2CON(OH); 1; Supplementary Table S5) are not distinguishable in the spectrum since the fundamentals of N-hydroxyoxaziridine (c-H2CON(OH); 1) either overlay with infrared absorptions of the reactants or are too weak to be observed.

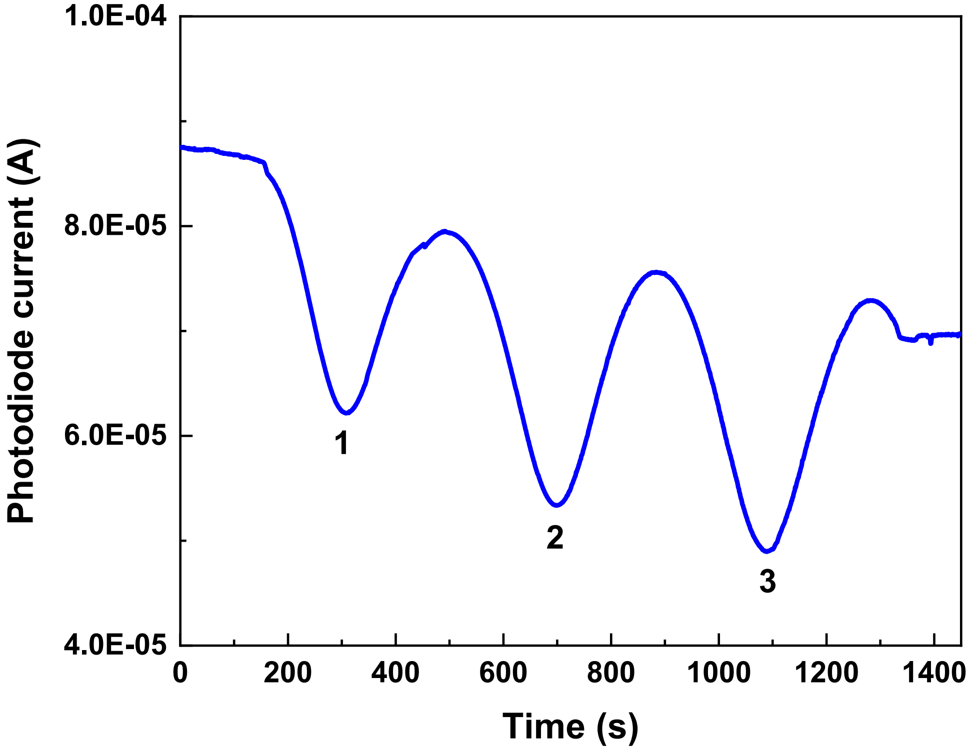

Figure S4. Interference pattern measured during the deposition of a $CH_4 + NO_2$ gas mixture for a 632.8 nm laser at an angle of incidence of 4°. Number of fringes are labelled below the signal minima.

The thickness of the ice (d) was determined using laser interferometry. A He-Ne laser of 632.8 nm has been used at an angle of incidence (θ) equal to 4° to measure the interference. The interference pattern observed during deposition of ice mixture is shown in Figure S3.

The refractive indices ($n = 1.32$)[4] of nitrogen dioxide and methane ice ($n = 1.33$) are very similar; therefore a refractive index value of $n = 1.32$ was considered in equation (1) to determine the thickness of the ice. The number of fringes (m) observed during the deposition of ice is equal to 3.

$$d = \frac{m\lambda}{2\sqrt{n^2 - \sin^2\theta}} \qquad (1)$$

where $\lambda = 632.8$ nm and $\theta = 4°$.

The ice composition was determined based on the column density of NO_2 and CH_4 measured via FTIR bands. The column density of NO_2, measured at the 1613 cm^{-1} band, $2.35 \pm 0.3 \times 10^{17}$ molecules cm^{-2}, and that of CH_4, determined at the 1297 cm^{-1} band, $2.83 \pm 0.2 \times 10^{17}$, molecules cm^{-2} indicate that the deposited ice mixture had a 1.2±0.1:1.0 CH_4 to NO_2 ratio.

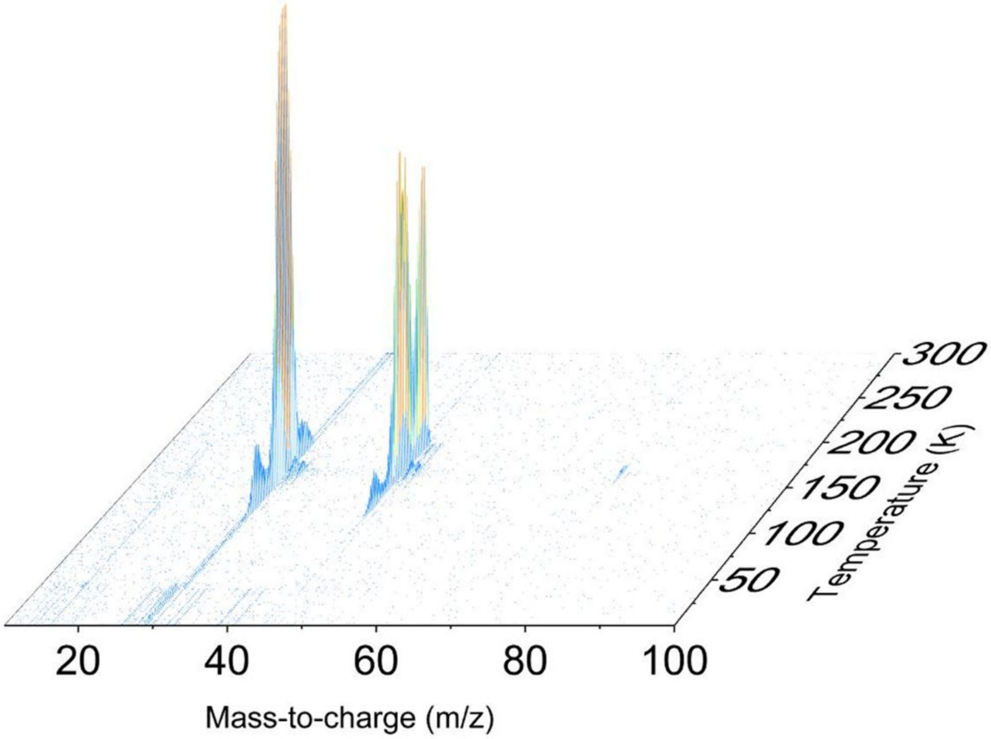

Figure S5. PI-ReTOF-MS data of the molecules subliming from a non-irradiated CH_4-NO_2 ice mixture as a function of temperature at a photon energy of 10.49 eV.

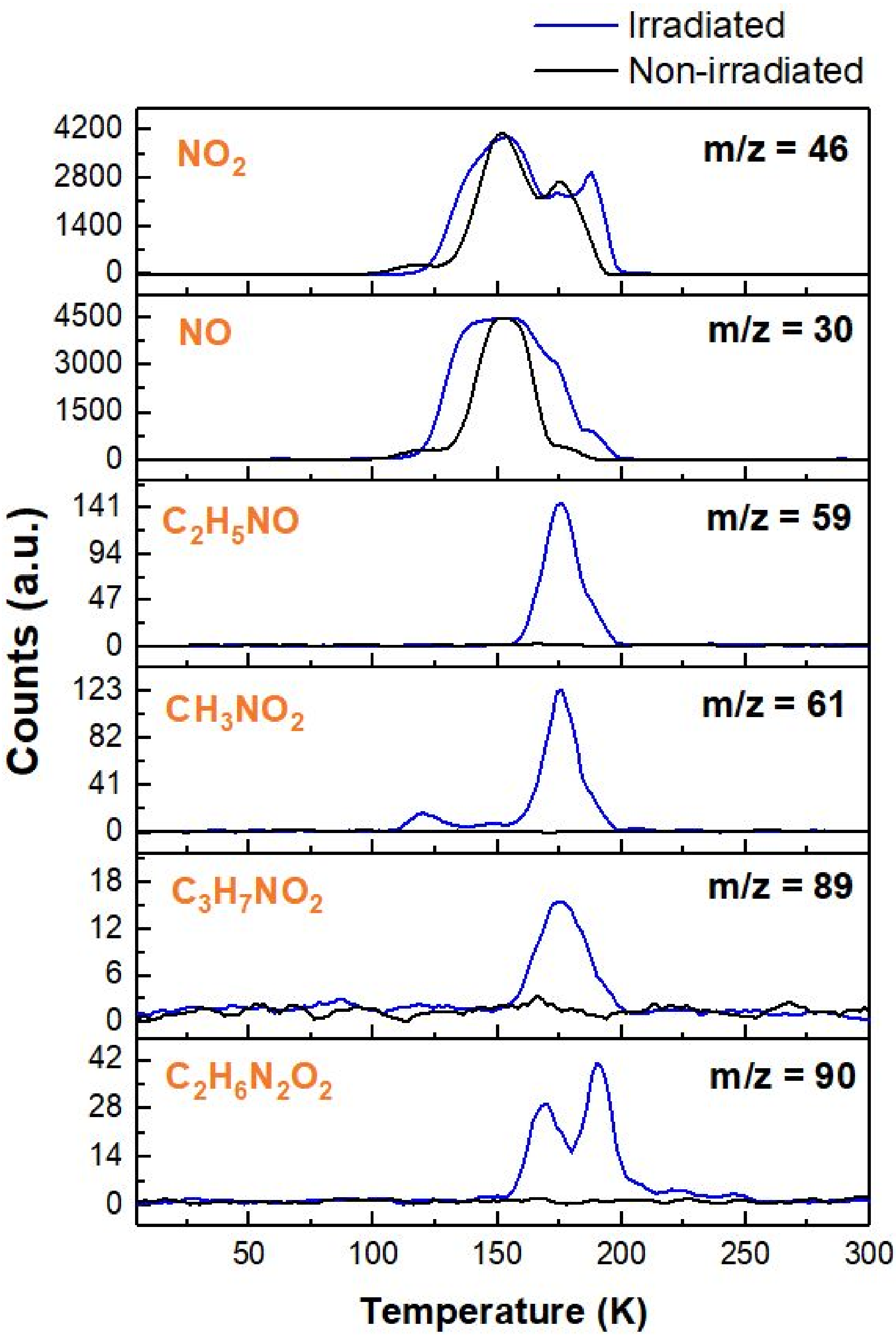

Figure S6. Temperature program desorption (TPD) profiles of molecules subliming from the irradiated and non-irradiated ice mixture. Parent molecule (nitrogen dioxide; NO_2) is measured at m/z = 46. All the product masses, measured at m/z = 59 (C_2H_5NO), 61 (CH_3NO_2), 89 ($C_3H_7NO_2$) and 90 ($C_2H_6N_2O_2$), are observed only in the case of irradiated ice mixture except m/z = 30 (nitrogen monoxide, NO). Nitrogen monoxide (m/z = 30; NO) is observed even in non-irradiated ice mixture due to photo-fragmentation of subliming NO_2 (nitrogen dioxide) molecules.

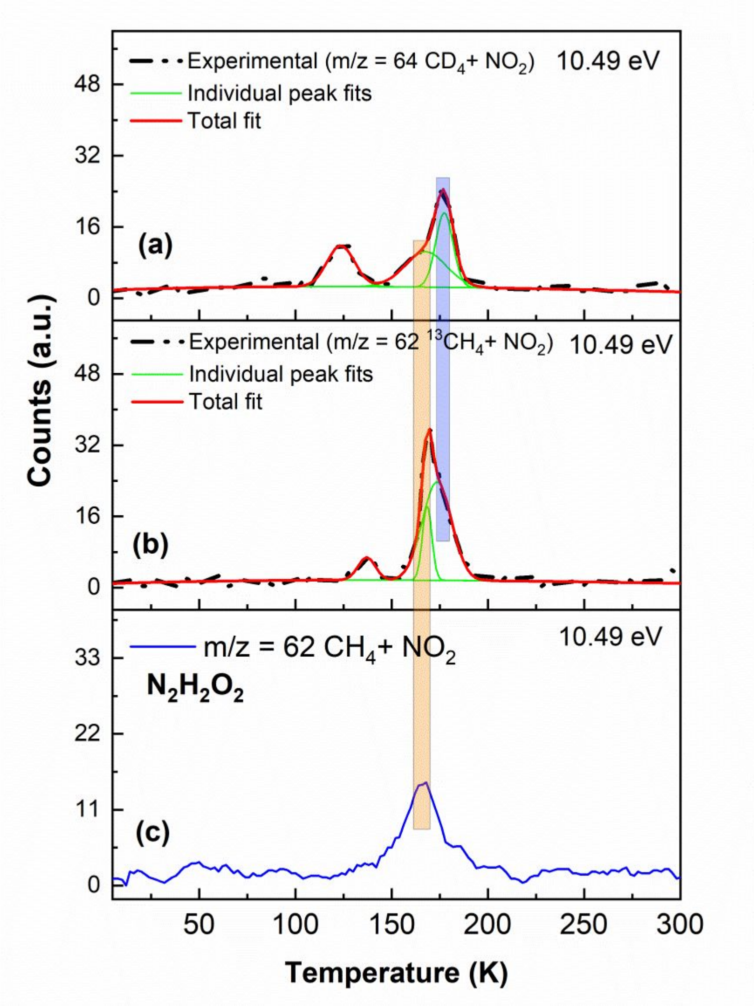

Figure S7. Temperature program desorption (TPD) profiles measured at (a) m/z = 64 in CD_4 + NO_2 system and (b) m/z = 62 in $^{13}CH_4$ + NO_2 system. (c) TPD profile measured at m/z = 62 in non-isotopic labeled CH_4 + NO_2 experiment; this ion signal corresponds to species of a molecular formula $N_2H_2O_2$ and contribute to ion counts at m/z = 64 and 62 in D4-methane and ^{13}C-labeled isotopic experiments in the temperature range 150-160 K (denoted by shaded orange bar). The peak corresponding to CH_3NO_2 molecular formula (plus isotopically labelled species) are denoted by shaded blue color bar.

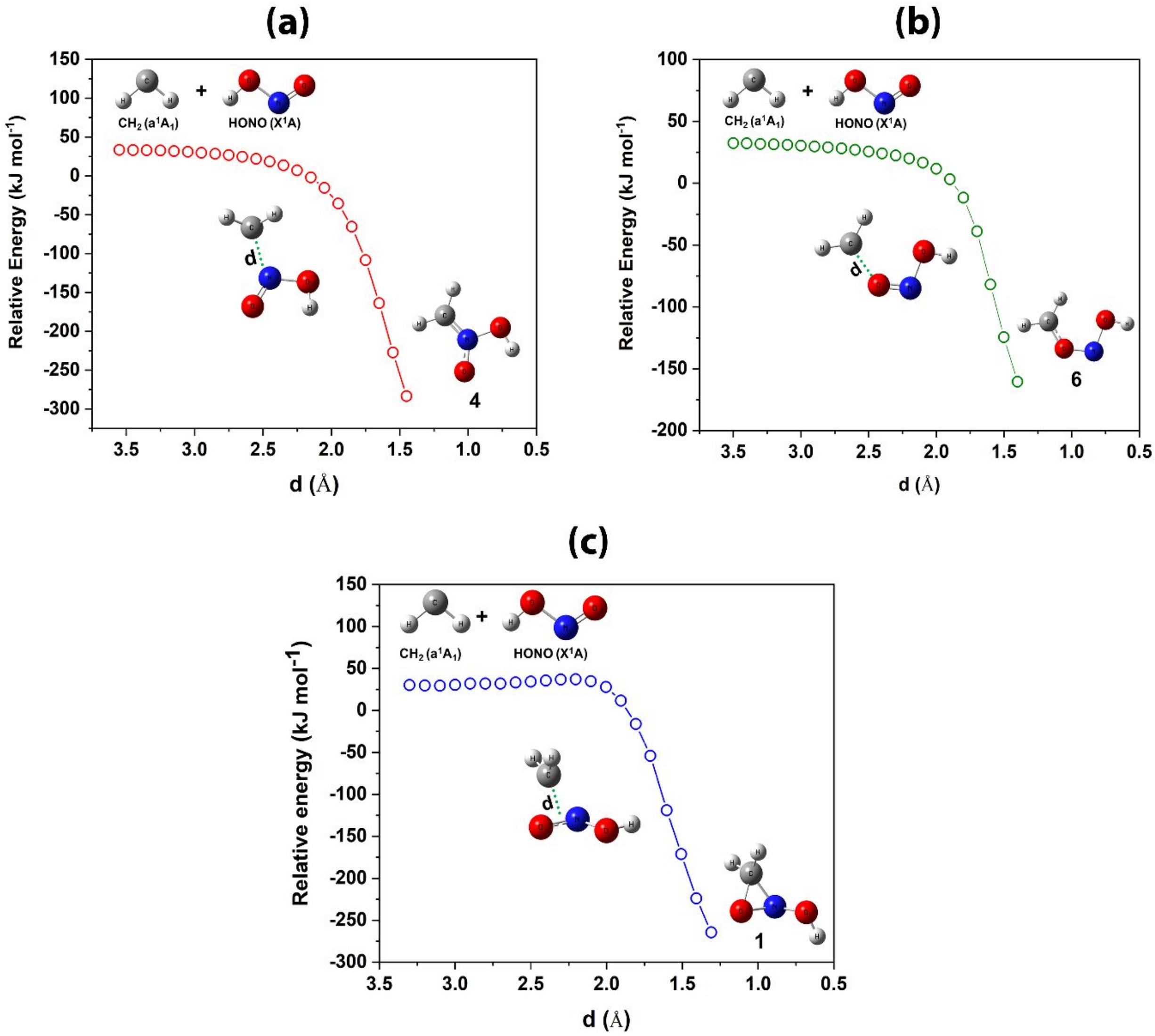

Figure S8. Intrinsic reaction coordinate (IRC) calculations at the CCSD/cc-pVTZ//CCSD (T)/CBS level of theory, for the formation of isomers (a) **4**, (b) **6,** and (c) **1** via addition of singlet carbene (CH_2) to nitrous acid (HONO). Barrier-less addition of carbene to the central nitrogen atom and to the terminal oxygen atom of HONO leads to isomers **4** and **6**, respectively. Isomer **1** can be formed via addition of singlet carbene to the N=O bond of nitrous acid, which has a small barrier of about 7 kJ mol^{-1}.

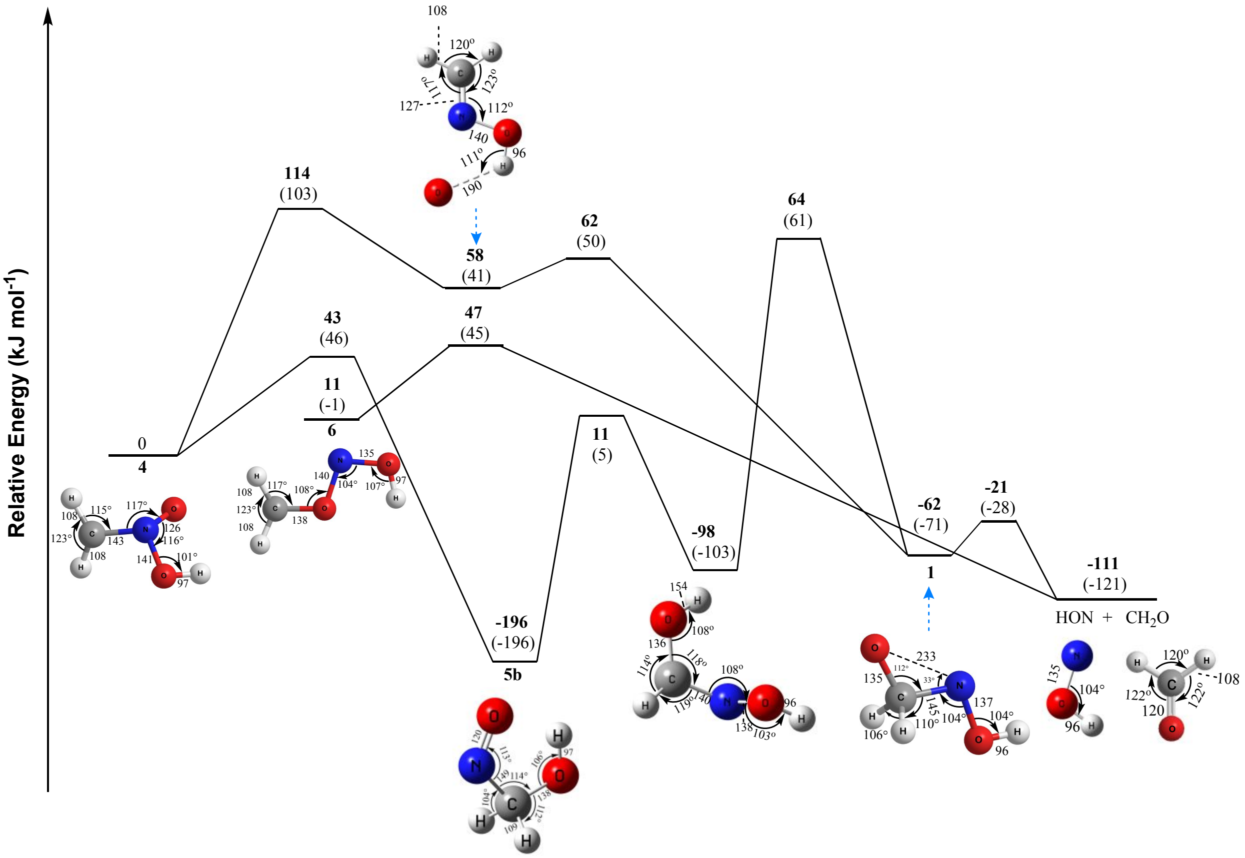

Figure S9. Formation pathway of triplet N-hydroxyoxaziridine (c-$H_2CON(OH)$; **1**) from triplet aci-nitromethane ($H_2CN(OH)O$; **4**), calculated at the CCSD(T)/CBS level of theory. Relative energies in parentheses are calculated at the CCSD/cc-pVTZ//MRCI/CBS level. Cartesian coordinates of the structures are provided in Table S10. Bond lengths and bond angles are given in picometers and degrees respectively.

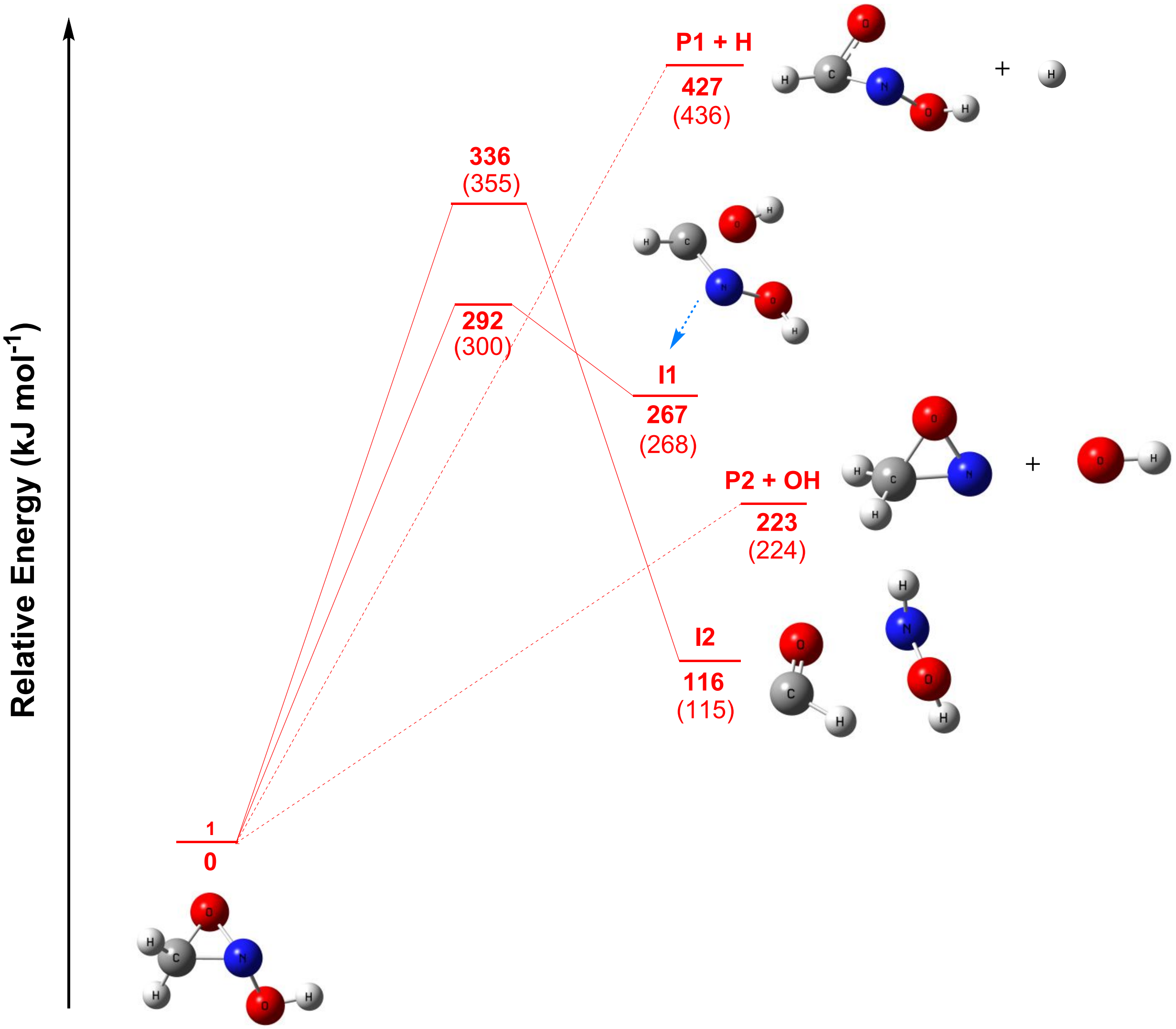

Figure S10. Unimolecular decomposition pathways of singlet N-hydroxyoxaziridine (c-$H_2CON(OH)$; **1**), calculated at the CCSD/cc-pVTZ//CCSD(T)/CBS level. Energies computed at the CCSD/cc-pVTZ//MRCI/CBS level are provided in parentheses. Cartesian coordinates of the structures are provided in Tables S9-S10. Note for those paths in dotted lines, the attempts are not made or not successful in locating the transition states.

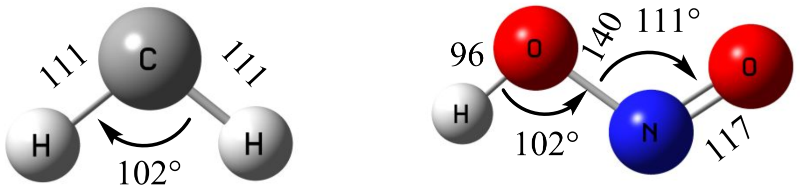

singlet CH_2 (a^1A_1)   singlet HONO (X^1A)

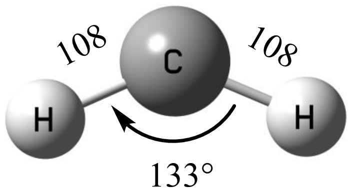

triplet CH_2 (X^3B_1)

Figure S11. Structures including geometrical parameters of singlet and triplet carbene (CH_2) along with singlet nitrous acid (HONO). Bond lengths are in pm and bond angles are in degrees.

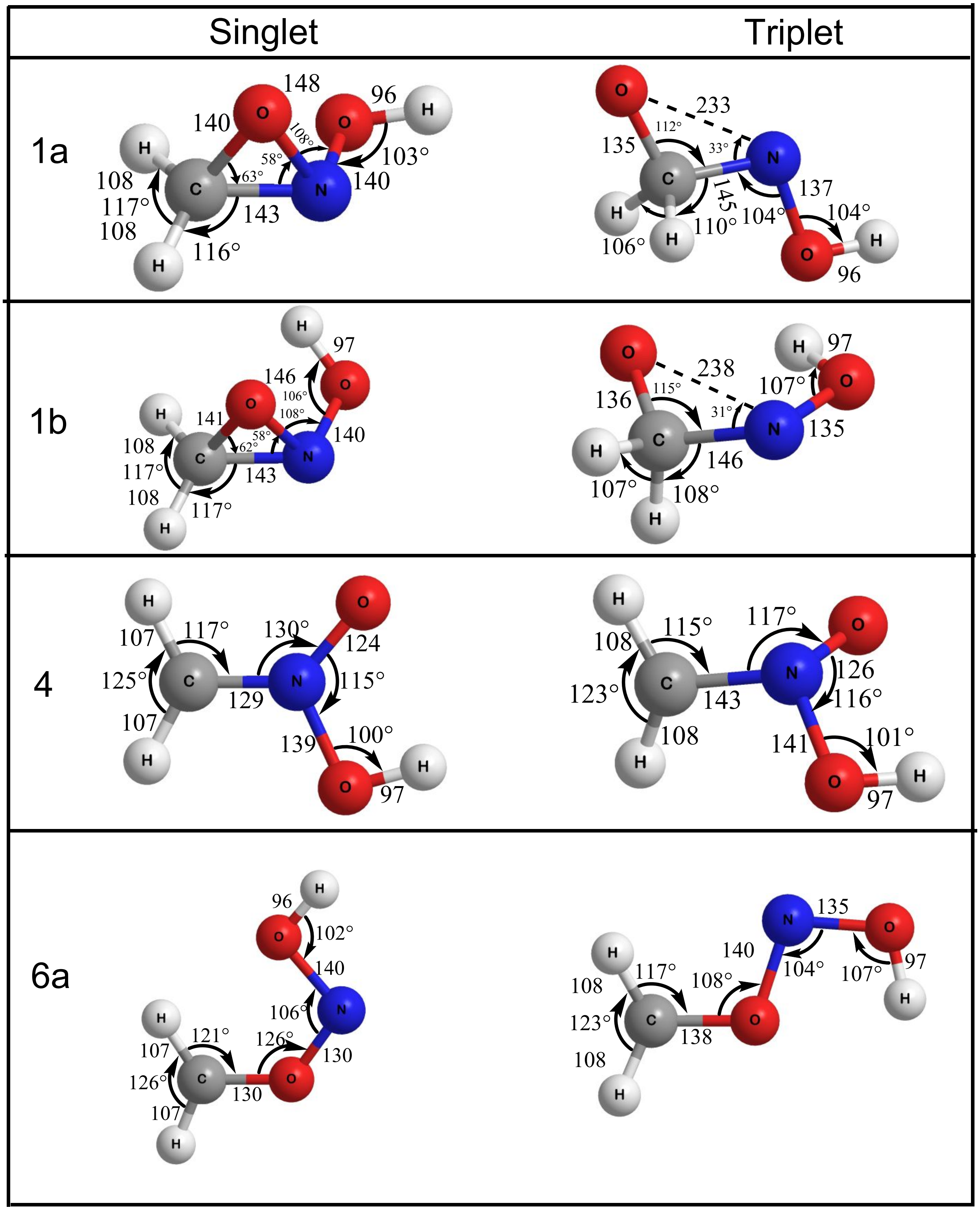

Figure S12. Structures along with geometrical parameters of 1a, 1b, 4, and 6a. Bond lengths are in pm and bond angles are in degrees.

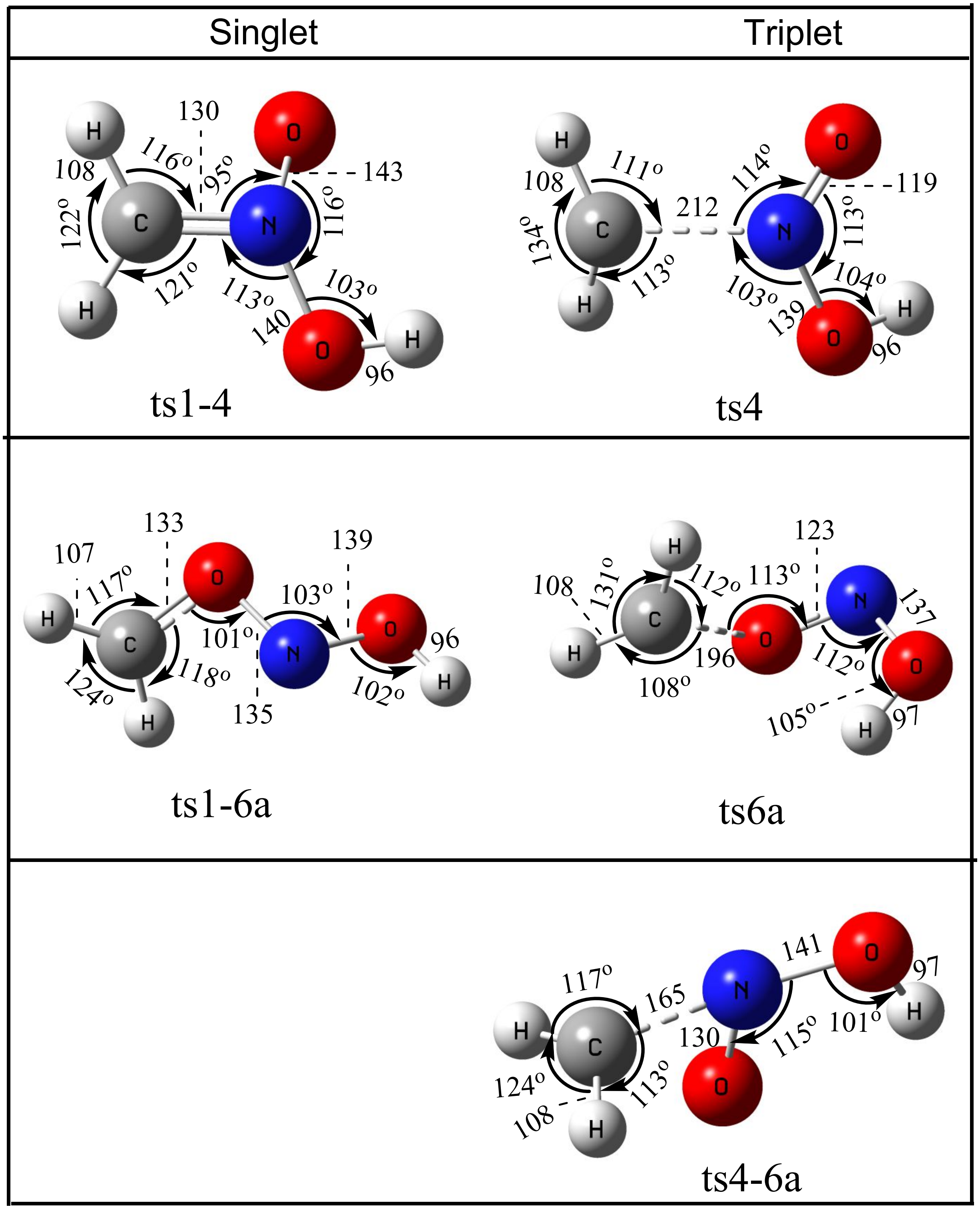

Figure S13. Structures and geometrical parameters of transition states corresponding to Fig. 4. Bond lengths are in pm and bond angles are in degrees.

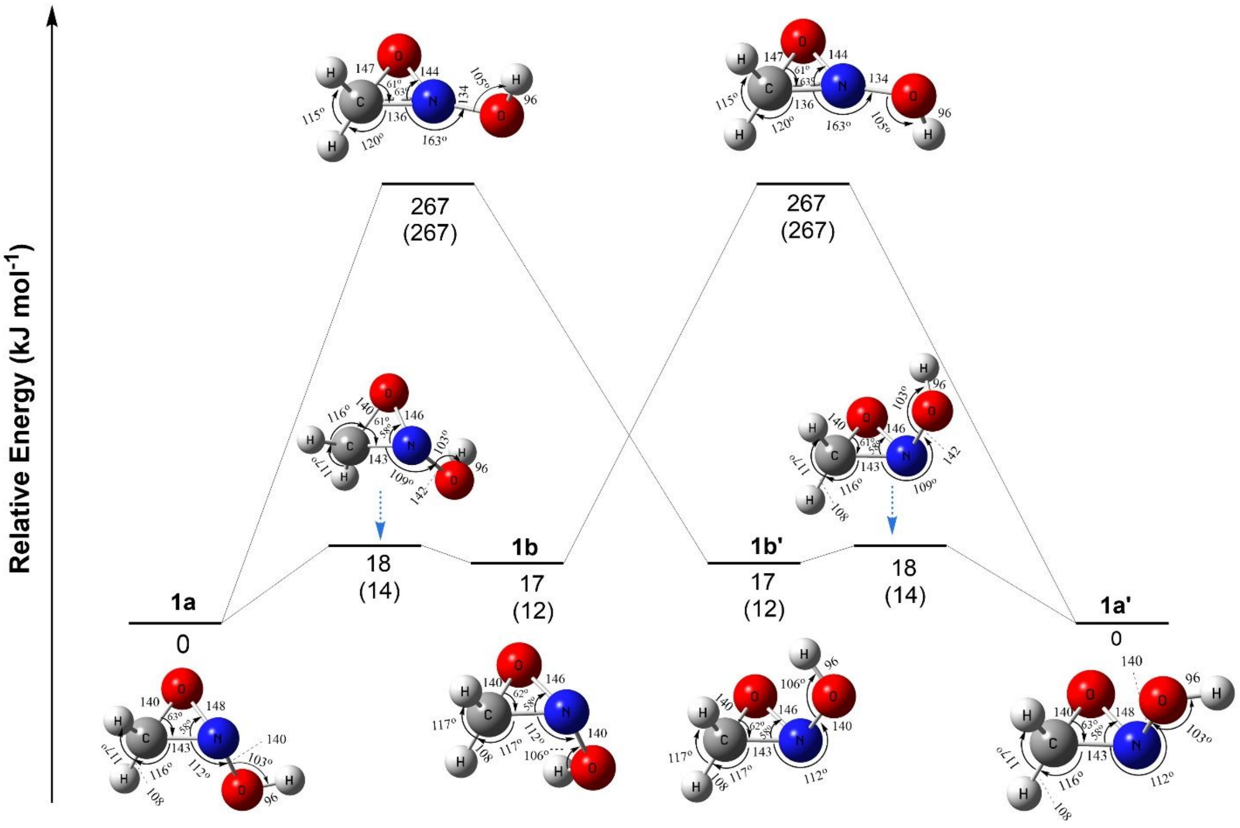

Figure S14. Computed (CCSD/cc-pVTZ//CCSD(T)/CBS level) isomerization processes of trans (**1a**/**1a'**) and cis (**1b**/**1b'**) conformers of N-hydroxyoxaziridine (c-$H_2CON(OH)$; **1**) along with ring inversion barriers. Relative energies in parentheses are calculated at the CCSD/cc-pVTZ//MRCI/CBS level. Bond lengths are in pm and bond angles are in degrees. Cartesian coordinates of the structures are provided in Tables S9- S10.

Table S1. (a) Infrared absorption features of CH_4 and NO_2 ice mixture before irradiation and (b) new absorption bands observed in the infrared spectrum after irradiation. All measurements have been performed at 5K.

(a) Before Irradiation			
Wavenumber Observed (cm^{-1})	Wavenumber Literature (cm^{-1})[4, 13,7]	Vibrational Assignments	Vibrational Modes
4530	4534	$\nu_2+\nu_3$	CH_4 combination
4300	4303	$\nu_3+\nu_4$	CH_4 combination
4204	4203	$\nu_1+\nu_4$	CH_4 combination
3010	3012	ν_3	CH_4 antisymmetric stretch
2904	2906	ν_1	CH_4 symmetric stretch
2815	2821	$\nu_2+\nu_4$	CH_4 combination
2040	-	$\nu_9+\nu_{12}$	N_2O_4 combination
1951	-	$\nu_1+\nu_4$	NO_2 combination
1860	1860	$\nu_4+\nu_5$	N_2O_4 combination
1737	1736	ν_9	N_2O_4 stretch
1608	1613	ν_3	NO_2 stretch
1297	1297	ν_4	CH_4 deformation
1257	1262	ν_{11}	N_2O_4 deformation
752	751	ν_{12}	N_2O_4 deformation
(b) After Irradiation			
2136	2137	ν_1	CO stretch
1694	1699	ν_2	HONO
1440	1430		CH_3 Deformation

Table S2. (a) Infrared absorption features of $^{13}CH_4$ and NO_2 ice mixture before irradiation and (b) new absorption bands observed in the infrared spectrum after irradiation. All measurements have been performed at 5K.

Wavenumber Observed (cm^{-1})	Wavenumber Literature (cm^{-1})[4, 15]	Vibrational Assignments	Vibrational Modes
(a) Before Irradiation			
4520	4534	$\nu_2+\nu_3$	$^{13}CH_4$ combination
4283	4301	$\nu_3+\nu_4$	$^{13}CH_4$ combination
4192	4213	$\nu_1+\nu_4$	$^{13}CH_4$ combination
2998	3009	ν_3	$^{13}CH_4$ antisymmetric stretch
2902	-	ν_1	$^{13}CH_4$ symmetric stretch
2807	2822	$\nu_2+\nu_4$	$^{13}CH_4$ combination
2040	-	$\nu_9+\nu_{12}$	N_2O_4 combination
1951	-	$\nu_1+\nu_4$	NO_2 combination
1862	1860	$\nu_4+\nu_5$	N_2O_4 combination
1737	1736	ν_9	N_2O_4 stretch
1608	1613	ν_3	NO_2 stretch
1291	-	ν_4	$^{13}CH_4$ deformation
1257	1262	ν_{11}	N_2O_4 deformation
752	751	ν_{12}	N_2O_4 bend
(b) After Irradiation			
2111	2100	ν_1	^{13}CO stretch
1690	1699	ν_2	HONO
1436	1430		$^{13}CH_3$ Deformation

Table S3. (a) Infrared absorption features of CD_4 and NO_2 ice mixture before irradiation and (b) new absorption bands observed in the infrared spectrum after irradiation. All measurements have been performed at 5K.

(a) Before Irradiation			
Wavenumber Observed (cm^{-1})	Wavenumber Literature (cm^{-1})[4, 16]	Vibrational Assignments	Vibrational Modes
4474	4478	$2\nu_3$	CD_4 Overtone
3237	3237	$\nu_3+\nu_4$	CD_4 combination
3089	3090	$\nu_1+\nu_4$	CD_4 combination
2970	-	$\nu_9+\nu_{11}$	N_2O_4 combination
2250	2252	ν_3	CD_4 antisymmetric stretch
2200	-	ν_1	N_2O stretch
2080	2073	ν_1 / $\nu_9+\nu_{12}$	CD_4 symmetric stretch or /and NO_2 combination
1970	1975	$2\nu_4$ / $\nu_1+\nu_4$	CD_4 overtone or/and NO_2 combination
1868	1860	$\nu_4+\nu_5$	N_2O_4 combination
1762	1763	ν_8	N_2O_4 stretch
1738	1736	ν_9	N_2O_4 stretch
1608	1613	ν_3	NO_2 stretch
1436	-		N_2O_4 deformation
1304	1304	ν_1	NO_2 stretch
1259	1262	ν_{11}	N_2O_4 deformation
989	990	ν_4	CD_4 bend
752	751	ν_{12}	N_2O_4 bend
(b) After Irradiation			
2167	2137	ν_1	CO stretch
1683	-	ν_2	DONO

Table S4. Data applied to calculate the average dose per molecule.

Initial Kinetic energy of the electrons	5 keV
Irradiation current (I)	20 ± 2 nA
Irradiation time (t)	900 s
Average penetration depth, l	289±30 nm
Average kinetic energy of backscattered electrons, E_{bs}[a]	3.8 ± 0.3 keV
Fraction of backscattered electrons, f_{bs}[a]	0.37 ± 0.03
Average kinetic energy of transmitted electrons, E_{trans}[a],	0.0 keV
Fraction of transmitted electrons, f_{trans}[a]	0
Density of the ice, ρ	1.17 g cm^{-3}
Irradiated area, A	1.0 ± 0.2 cm^2
total number of molecules processed	$(3.3 \pm 0.3) \times 10^{17}$
dose per molecule, D	1.2 ± 0.2 eV
Total number of electrons	$(1.1 \pm 0.1) \times 10^{14}$

[a] Values from CASINO simulations.

Table S5. The calculated anharmonic frequencies of the N-hydroxyoxaziridine (c-H_2CON(OH); **1**).

	Calculated		Assignments
Normal modes	Anharmonic frequencies (cm^{-1})	Intensity (km mol^{-1})	
ν1	353	111	
ν2	455	26	
ν3	490	1	
ν4	627	92	Ring vibration
ν5	813	19	Ring vibration
ν6	939	38	Ring asymm. stretch
ν7	1067	8	CH_2 deformation
ν8	1136	4	
ν9	1182	3	
ν10	1236	50	CH_2 wagging
ν11	1386	37	N-O-H bending
ν12	1485	3	C-H bending
ν13	2900	19	Symm. C-H stretch
ν14	3016	20	Asymm. C-H stretch
ν15	3600	61	O-H stretch

Table S6. Calculated (B3LYP//CCSD(T)/CBS level) and experimental ionization energies (IE) of the CH_3NO_2 isomers.

Isomers		Ionization energies (IE, eV)	
		Calculated	Experimental
1a	*trans*-N-hydroxyoxaziridine	9.99	-
1b	*cis*-N-hydroxyoxaziridine	9.79	-
2	Nitromethane	11.10	11.08[13]
3a	*cis*-methylnitrite	10.50	-
3b	*trans*-methylnitrite	10.31	10.38[14]
4a	*trans*-aci-nitromethane	9.57	-
4b	*cis*-aci-nitromethane	9.56	-
5a	*trans*-nitrosomethanol	8.77	-
5b	*cis*-nitrosomethanol	8.90	-
6a	*cis*-hydroxy(methyleneoxonio)amide	8.18	-
6b	*trans*-hydroxy(methyleneoxonio)amide	7.79	-
7a	*cis*-formohydroxamic acid	9.50	-
7b	*trans*-formohydroxamic acid	9.65	-
8a	*cis*-N-hydroxyformimidic acid	9.66	-
8b	*trans*-N-hydroxyformimidic acid	9.42	-
9a	*trans*-N-oxido-N-hydroformimidic acid	8.38	-
9b	*cis*-N-oxido-N-hydroformimidic acid	8.47	-
10a	*trans*-carbamic acid	10.58	-
10b	*cis*-carbamic acid	10.74	-
11	Carbonimidic acid	9.94	-
12	1,2,3-dioxazetidine	9.20	-
13	1,3,2-dioxazetidine	9.04	-
14a	trans-(aminooxy)formaldehyde	9.48	-
14b	cis-(aminooxy)formaldehyde	9.39	-
15	3-methyl-1,2,3-dioxaziridine	10.71	-

Table S7. Experimental and calculated ionization energies of various molecules.

Name	Structure	Ionization energy (eV)		
		B3LYP//CCSD (T)/CBS	Exp.	Error
Nitrosomethane[1]	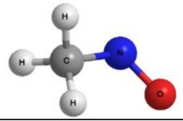	**9.25**	**9.3**[a]	+0.05
Trans-Formaldehyde oxime[1]	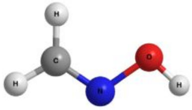	**10.03**	**10.11**[a]	+0.08
Nitromethane	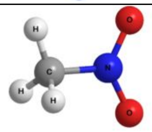	**11.10**	**11.08** [b]	-0.02
Trans-methyl nitrite[1]	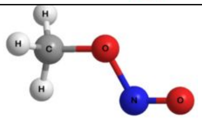	**10.31**	**10.38** [c]	+0.07
Trans-nitrosomethane dimer[1]	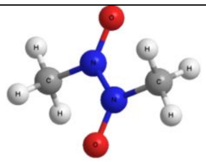	**8.38**	**8.3** [a]	-0.08
N-methyl formamide[2]	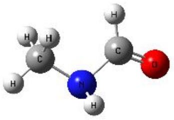	**9.80**	**9.83** [d]	-0.03
Acetamide[2]	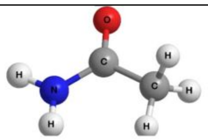	**9.74**	**9.69** [d]	-0.05
Metanimine[3]	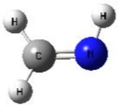	**9.94**	**9.88** [e]	-0.06
1,1-Dimethylhydrazine[3]	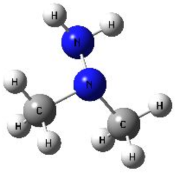	**7.24**	**7.29** [f]	-0.05
Formamide[4]	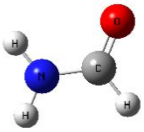	**10.24**	**10.16** [d]	-0.08

[a]Frost, D.C.; Lau, W.M.; McDowell, C.A.; Westwood, N.P.C. A Study by He I Photoelectron Spectroscopy of Monomeric Nitrosomethane, the Cis and Trans Dimers, and Formaldoxime. *J. Phys. Chem*. **1982**, *86*, 3577. [b]Lifshitz, C.; Rejwan, M.; Levin, I.; Peres, T., Unimolecular Fragmentations of the Nitromethane Cation. *Int. J. Mass Spectrom. Ion Processes* **1988**, *84*, 271. [c]Gilman, J.P.; Hsieh, T.; Meisels, G.G. Competition Between Isomerization and Fragmentation of Gaseous Ions. II. Nitromethane and methylnitrite ion*s*. *J. Chem. Phys.* **1983**, *78*, 1174. [d]National Institute of Standards and technology (NIST) U.S. Department of Commerce. [e]Tarasenko, N.A.; Tishenkov, A.A.; Zaikin, V.G.; Volkova, V.V.; Gusel'nikov, L.E. Adiabatic Ionization Energy of Methylenimine. *Bull. Acad. Sci. USSR, Div. Chem. Sci.* **1986**, *10*, 2196. [f]Mautner, M.; Nelsen, S.F.; Willi, M.R.; Frigo, T.B. Special Effects of an Unusually Large Neutral to Radical Cation Geometry Change. Adiabatic Ionization Energies and Proton Affinities of Alkylhydrazines. *J. Am. Chem. Soc.* **1984**, *106*, 7384. [1]Calculated ionization energy values taken from reference Maksyutenko, P.; Förstel, M.; Crandall, P.; Sun, B.-J.; Wu, M.-H.; Chang, A. H. H.; Kaiser, R. I. An Isomer-Specific Study of Solid Nitromethane Decomposition Pathways – Detection of Aci-nitromethane ($H_2CNO(OH)$) and Nitrosomethanol ($HOCH_2NO$) Intermediates. *Chem. Phys. Lett.* **2016**, *658*, 20-29.[2]Calculated values reproduced from reference Frigge, R.; Zhu, C.; Turner, A. M.; Abplanalp, M. J.; Bergantini, A.; Sun, B.-J.; Chen, Y.-L.; Chang, A. H. H.; Kaiser, R. I. A Vacuum Ultraviolet Photoionization Study on the Formation of N-methyl Formamide ($HCONHCH_3$) in Deep Space: A Potential Interstellar Molecule with a Peptide Bond. *ApJ.* **2018,** *862*, 84.[3]Calculaed values reproduced from reference Zhu, C.; Frigge, R.; Turner, A. M.; Abplanalp, M. J.; Sun, B.-J.; Chen, Y.-L.; Chang, A. H. H.; Kaiser, R. I., A Vacuum Ultraviolet Photoionization Study on the Formation of Methanimine (CH_2NH) and Ethylenediamine ($NH_2CH_2CH_2NH_2$) in Low Temperature Interstellar Model Ices Exposed to Ionizing Radiation. *Phys. Chem. Chem. Phys.* **2019**, *21*, 1952-1962.[4]Calculaed values reproduced from reference Förstel, M.; Maksyutenko, P.; Jones, B. M.; Sun, B. J.; Lee, H. C.; Chang, A. H. H.; Kaiser, R. I., On the Formation of Amide Polymers via Carbonyl–Amino Group Linkages in Energetically Processed Ices of Astrophysical Relevance. *ApJ.* **2016**, *820*, 117.

The ionization energies derived from CCSD(T)/CBS with B3LYP/cc-pVTZ zero point correction method have overall error range of ± 0.08 eV with respect to the experimental ionization energies.

Generation of VUV light

1. 10.49 eV –The third harmonics (355 nm) of a pulsed ND:YAG laser (Spectra Physics, PRO-250-30; 30 Hz) is exploited for generating 10.49 eV VUV light. The 355 nm light is focused on pulsed jet of Xenon (80 μs, 30 Hz) which results in generation of 118 nm light (10.49 eV) via non-linear mixing. The 10.49 eV light is separated from 355 nm light by a LiF biconvex lens (ISP Optics) and directed 2 mm above the sample to ionize the subliming molecules.

2. 10.20 eV – The second harmonics (532 nm) of a pulsed ND:YAG laser (Spectra Physics, PRO-250-30; 30 Hz, 10 ns) is used to pump a dye laser (Sirah Cobra Stretch) having Rhodamine 610/640 dye mixture. The fundamental output of the dye laser (607 nm) undergoes frequency tripling to generate 202 nm (ω1). Two photons of ω1 is required to accesses the resonant transition of Krypton. The 532 nm light from a second ND:YAG laser (Spectra Physics, PRO-250-30; 30 Hz, 10 ns) is used to pump another dye laser (Sirah Cobra Stretch) containing Rhodamine 610/640 dye mixture to generate 606 nm (ω2) light. The 202 nm and 606 nm lights are spatially and temporally overlapped on pulsed jet of Krypton (80 μs, 30 Hz) which act as a non-linear medium. Difference frequency mixing of two photons of ω1 and one photon of ω2 in Krypton (2ω1-ω2) results in the generation of 121.5 nm (ω_{VUV}; 10.20 eV) light. A LiF biconvex lens is used to separate the 121.5 nm light from residual 202 and 606 nm lights.

3. 9.80 eV – The 126.51 nm (9.80 eV) light is generated via difference frequency mixing of two photons of 202 nm (ω1) and one photon of 504.7 nm (ω2) in krypton. The process of producing 202 nm has been discussed in the generation of 10.20 eV light. To generate 504.7 nm light, a dye laser containing Coumarin 503 dye is being pumped by the third harmonics (355 nm) of a ND:YAG laser. The 202 nm (ω1) and 504.7 nm (ω2) lights are spatially and temporally overlapped on pulsed jet of Krypton for difference frequency generation of 9.80 eV light, which is eventually separated from the residual ω1 and ω2 through a LiF biconvex lens. The generated 9.80 eV light is directed at about 2 mm above the sample to ionize the subliming molecules.

4. 9.70 eV – Difference frequency mixing of two photons of 202 nm (ω1) and one photon of 485 nm (ω2) in Krypton results in generation of 127.8 nm (9.70 eV) light. The process of producing 202 nm is identical to that of described in the generation of 10.20 eV light. To generate 485 nm light, a dye laser containing Coumarin 480 dye is being pumped by the third harmonics (355 nm) of a ND:YAG laser. Both ω1 and ω2 are spatially and temporally overlapped on pulsed jet of

Krypton for difference frequency generation of 127.8 nm light. The 127.8 nm light generated is eventually separated from the residual 202 nm and 485 nm lights by the help of LiF biconvex lens and directed at about 2 mm above the sample to ionize the subliming molecules.

Table S8. Parameters for the Vacuum Ultraviolet Light (VUV) generation in the present study.

		ω1				ω2			
VUV Energy	Noble gas	YAG 1 (λ; nm)	Dye	Dye laser (λ; nm)	Wavelength after tripling (nm)	YAG 2 (λ; nm)	Dye	Dye laser (λ; nm)	Photons/pulse*
10.49 eV	Xe	355	-	-	-	-	-	-	10^{14}
10.20 eV	Kr	532	Rhodamine 610/640	606.94	202.31	532 nm	Rhodamine 610/640	606	10^{14}
9.80 eV	Kr	532	Rhodamine 610/640	606.94	202.31	355 nm	Coumarin 503	504.7	10^{14}
9.70 eV	Kr	532	Rhodamine 610/640	606.948	202.31	355 nm	Coumarin 480	485	10^{14}

* 30 Hz

Table S9. Optimized geometrical co-ordinates of CH_3NO_2 isomers depicted in **Figure 1**

Atom	X	Y	Z	Atom	X	Y	Z
1a				**1b**			
C	0.886630	0.607560	-0.067750	C	0.891092	-0.599108	0.115372
H	1.660592	1.008439	0.581228	H	1.719855	-0.980089	-0.467948
H	0.654893	1.185008	-0.957892	H	0.645019	-1.137694	1.023435
O	0.823328	-0.783875	-0.199833	O	0.745243	0.799084	0.159670
N	-0.212101	-0.030758	0.584256	N	-0.190767	-0.013516	-0.613361
O	-1.345009	0.141365	-0.231494	O	-1.395468	-0.086339	0.094124
H	-1.977110	-0.483420	0.143985	H	-1.174254	0.105087	1.015461
2				**3a**			
C	-1.323754	0.000628	-0.003415	C	1.325951	0.332716	0.000000
H	-1.662214	0.908829	-0.488488	H	1.984972	1.194885	0.000000
H	-1.632081	-0.008988	1.039678	H	1.491034	-0.277194	0.887654
H	-1.663517	-0.897955	-0.505448	H	1.491034	-0.277194	-0.887654
N	0.175101	-0.000088	-0.009105	O	0.000000	0.886104	0.000000
O	0.729030	-1.084952	0.002437	N	-1.045702	-0.047976	0.000000
O	0.730298	1.084322	0.002373	O	-0.700354	-1.173725	0.000000
3b				**4a**			
C	-1.415241	0.839957	0.000000	C	1.238765	0.506734	0.000000
H	-1.927028	-0.122307	0.000000	H	1.422838	1.565125	0.000000
H	-1.687889	1.404124	0.890923	H	2.002884	-0.247231	0.000000
H	-1.687889	1.404124	-0.890923	N	0.000000	0.129342	0.000000
O	0.000000	0.637028	0.000000	O	-1.041154	0.790466	0.000000
N	0.305280	-0.758702	0.000000	O	-0.173423	-1.281091	0.000000
O	1.457162	-0.938874	0.000000	H	-1.141703	-1.338691	0.000000

4b				**5a**			
O	1.239383	-0.420826	-0.001804	C	0.000000	0.861009	0.000000
H	1.149652	-1.383889	0.014649	H	-0.252137	1.457108	0.888030
N	-0.095665	0.108756	-0.000051	H	-0.252137	1.457108	-0.888030
O	-0.119951	1.324213	0.000534	O	1.301506	0.370945	0.000000
C	-1.080262	-0.744792	-0.000298	H	1.916224	1.110140	0.000000
H	-2.073803	-0.335101	0.002068	N	-1.024912	-0.217801	0.000000
H	-0.880076	-1.800646	-0.004411	O	-0.581201	-1.329170	0.000000
5b				**6a**			
C	0.000000	0.897655	0.000000	O	-1.183794	0.580039	-0.000046
H	-0.253238	1.495959	0.885622	H	-2.132922	0.411734	-0.000098
H	-0.253238	1.495959	-0.885622	N	-0.661208	-0.729638	0.000027
O	1.309963	0.470761	0.000000	O	0.636859	-0.598101	0.000020
H	1.272166	-0.502770	0.000000	C	1.320825	0.506032	0.000053
N	-1.015150	-0.191948	0.000000	H	0.828411	1.458872	0.000356
O	-0.517418	-1.287191	0.000000	H	2.383500	0.345165	-0.000559
6b				**7a**			
O	1.631855	0.270509	-0.012700	C	-0.775719	0.481150	-0.012211
H	2.334258	-0.381716	0.086754	H	-1.318168	1.436027	-0.057367
N	0.487198	-0.553141	-0.005585	O	-1.302864	-0.617194	-0.001139
O	-0.490711	0.313989	0.007493	N	0.562633	0.640157	0.085826
C	-1.740092	-0.026130	0.000886	O	1.345110	-0.513369	-0.012932
H	-2.012286	-1.069247	-0.015692	H	0.660383	-1.208058	-0.072378
O	1.631855	0.270509	-0.012700	H	1.035705	1.448539	-0.285206
7b				**8a**			
C	-0.680750	0.355799	0.041169	C	0.000000	0.882569	0.000000
H	-0.428378	1.426692	0.101580	H	-0.223909	1.939300	0.000000
O	-1.799675	-0.085881	-0.051994	O	1.307003	0.585208	0.000000
N	0.437672	-0.436275	0.147525	H	1.381769	-0.381498	0.000000
O	1.664696	0.173013	-0.173938	N	-0.969795	0.059271	0.000000
H	2.160630	0.169739	0.653120	O	-0.447759	-1.267947	0.000000
H	0.368377	-1.374355	-0.226935	H	-1.243247	-1.806200	0.000000

8b				**9a**			
C	0.000000	0.609872	0.000000	C	-0.479209	0.425447	-0.000666
H	-0.935413	1.157868	0.000000	H	-0.396210	1.500821	-0.048155
O	1.092090	1.397806	0.000000	H	0.424536	-1.311659	0.072985
H	1.872567	0.825573	0.000000	O	1.805613	0.096449	-0.010187
N	0.099929	-0.651309	0.000000	N	0.595774	-0.297261	0.030073
O	-1.176949	-1.258887	0.000000	O	-1.678367	-0.213609	-0.071839
H	-0.957791	-2.194859	0.000000	H	-2.341459	0.276262	0.424875
9a				**9b**			
C	-0.479209	0.425447	-0.000666	C	0.000000	0.811883	0.000000
H	-0.396210	1.500821	-0.048155	H	-0.402614	1.813213	0.000000
H	0.424536	-1.311659	0.072985	H	-1.812751	0.081445	0.000000
O	1.805613	0.096449	-0.010187	O	-0.552028	-1.434221	0.000000
N	0.595774	-0.297261	0.030073	N	-0.823405	-0.192480	0.000000
O	-1.678367	-0.213609	-0.071839	O	1.324847	0.579764	0.000000
H	-2.341459	0.276262	0.424875	H	1.796644	1.417061	0.000000
10a				**10b**			
O	0.848298	-0.968843	-0.001654	O	1.072284	0.749036	0.021805
H	1.750920	-0.626380	-0.004239	H	0.759144	1.633113	-0.199040
C	0.037020	0.125447	0.001377	C	0.051166	-0.152753	0.001499
O	0.449419	1.261131	-0.004053	O	0.265416	-1.332608	0.007206
N	-1.267449	-0.246806	0.032702	N	-1.207149	0.413453	-0.067262
H	-1.957945	0.470205	-0.086571	H	-1.954125	-0.249511	0.059933
H	-1.524679	-1.207166	-0.100711	H	-1.363574	1.307319	0.368854
11				**12**			
O	-0.751855	-1.060094	-0.000107	C	0.909804	0.293223	0.124530
H	-1.653933	-0.716883	-0.000174	H	1.250577	0.321128	1.161602
C	0.111623	-0.025592	0.000009	H	1.700829	0.585919	-0.566307
O	-0.548096	1.155082	-0.000009	O	0.322173	-0.986339	-0.186524
N	1.367448	-0.096743	0.000122	N	-0.375513	0.975236	-0.017115
H	0.125620	1.847053	0.000073	O	-0.980249	-0.344984	0.160334
H	1.686052	-1.059314	0.000117	H	-0.517027	1.157543	-1.013154

13				**14a**			
C	0.099547	0.950296	0.000000	O	-1.486320	-0.989692	0.000000
H	-0.818846	1.557087	0.000000	C	-0.350700	-0.637151	0.000000
H	0.991271	1.580766	0.000000	O	0.000000	0.677392	0.000000
O	0.099547	-0.030343	1.031932	N	1.410334	0.948421	0.000000
H	-1.195674	-1.099782	0.000000	H	1.796883	0.494308	0.824011
O	0.099547	-0.030343	-1.031932	H	0.528656	-1.306253	0.000000
N	-0.166683	-1.036336	0.000000	H	1.796883	0.494308	-0.824011
14b				**15**			
C	0.099547	0.950296	0.000000	O	0.148438	-0.872370	0.729266
H	-0.818846	1.557087	0.000000	N	-0.594967	0.104081	0.000000
H	0.991271	1.580766	0.000000	O	0.148438	-0.872370	-0.729266
O	0.099547	-0.030343	1.031932	C	0.148438	1.365866	0.000000
H	-1.195674	-1.099782	0.000000	H	-0.162470	1.917676	0.886846
O	0.099547	-0.030343	-1.031932	H	1.224067	1.198807	0.000000
N	-0.166683	-1.036336	0.000000	H	-0.162470	1.917676	-0.886846

Table S10. CCSD/cc-pVTZ optimized coordinates of reactants, intermediates, transition states, and products in the reactions of singlet and triplet carbene (CH_2) with nitrous acid (HONO). Coordinates of CPMCSCF/TZVPP optimized minimal-energy crossing points (MSX).

Cartesian coordinates of relevant reactants, complexes, transition states, and minimal-energy crossing points (MSX) of **Figure 4.**

Atom	X	Y	Z	Atom	X	Y	Z
singlet CH_2				**triplet CH_2**			
C	0.000000	0.000000	0.175281	C	0.000000	0.000000	0.106441
H	0.000000	0.859343	-0.525842	H	0.000000	0.989354	-0.319322
H	0.000000	-0.859343	-0.525842	H	0.000000	-0.989354	-0.319322
singlet HONO				**triplet 1**			
O	0.888952	-0.573744	0.000000	c	-0.703422	0.465188	0.217803
H	1.747459	-0.137658	0.000000	H	-1.243259	1.397994	-0.010050
N	0.000000	0.512897	0.000000	H	-0.637825	0.413238	1.326643
O	-1.107385	0.142167	0.000000	O	-1.422688	-0.609358	-0.169219
				N	0.628552	0.593146	-0.346559
				O	1.358026	-0.439684	0.176247
				H	2.219041	-0.36204	-0.253721

triplet 4				**triplet 6a**			
O	-1.027070	-0.811023	0.009968	O	1.672680	-0.054339	-0.015590
H	-1.770392	-0.208810	0.139225	H	1.480097	-1.002314	-0.018551
N	0.015116	0.091839	-0.269308	N	0.483301	0.578083	-0.005763
O	-0.159869	1.270735	0.125911	O	-0.457112	-0.456736	0.058947
C	1.278979	-0.509148	0.026934	C	-1.710965	0.094121	-0.085243
H	1.371889	-0.974763	0.997035	H	-1.826890	1.118835	0.229989
H	2.114329	-0.082108	-0.499731	H	-2.495065	-0.639226	-0.006497
triplet ts4				**triplet ts6a**			
O	0.784521	1.055004	0.003569	O	1.358500	0.629226	0.085943
H	1.437231	0.812348	0.679540	H	0.8442770	0.8812780	0.8701670
N	0.245961	-0.166839	-0.387405	N	0.7407560	-0.4963950	-0.3969530
O	0.733341	-1.097133	0.169115	O	-0.2611700	-0.7738770	0.2531190
C	-1.819564	0.086384	0.020554	C	-1.7514290	0.4552610	-0.0507180
H	-2.055446	1.037550	0.470569	H	-1.7086240	0.9058170	-1.0303620
H	-2.329025	-0.863298	0.056925	H	-2.5910110	0.1133040	0.5306780

triplet ts4-6a				**4-MSX**			
O	-1.566320	-0.303163	0.029730	O	1.008126	-0.530378	-0.465869
H	-1.764347	0.623849	0.237557	H	1.7490732	-0.5885061	0.1108797
N	-0.172762	-0.251306	-0.164302	N	0.0253574	0.1093553	0.2522229
O	0.369341	0.912340	0.025161	O	-0.0212526	1.3882566	-0.0093908
C	1.449965	-0.502892	0.030065	C	-1.2224616	-0.5364224	0.0365014
H	1.756998	-0.553093	1.060968	H	-1.3514064	-1.0361479	-0.9034760
H	2.092724	-0.167678	-0.767924	H	-2.0462176	-0.0654612	0.5281463
6a-MSX				**1-MSX**			
O	1.651271	-0.097475	-0.119926	C	0.832242	0.452835	-0.052223
H	1.483125	-1.019457	0.004990	H	1.480895	0.986852	0.628665
N	0.499985	0.564040	-0.061536	H	0.632456	1.040080	-0.940424
O	-0.461209	-0.394606	0.270534	O	1.405106	-0.762521	-0.474534
C	-1.684289	0.122761	-0.082975	N	-0.36895	0.104836	0.670622
H	-1.928696	1.081048	0.332958	O	-1.37034	0.078811	-0.21981
H	-2.429064	-0.637352	-0.191580	H	-2.12019	-0.25657	0.240203

singlet 1				**singlet 4**			
C	0.889995	0.603607	-0.064256	O	-0.139214	-1.268610	0.000000
H	1.676206	0.977975	0.580008	H	-1.103109	-1.335892	0.000000
H	0.649171	1.189807	-0.942470	N	0.000000	0.118699	0.000000
O	0.796848	-0.781783	-0.208125	O	-1.062436	0.754645	0.000000
N	-0.204439	-0.042106	0.583854	C	1.223365	0.535820	0.000000
O	-1.331231	0.154604	-0.225854	H	1.369356	1.599062	0.000000
H	-1.959215	-0.477251	0.132850	H	2.006763	-0.197267	0.000000
singlet 6a				**singlet ts1-4**			
O	1.164205	0.579670	0.000272	C	-0.766696	0.936488	0.032453
H	2.110691	0.419643	-0.000218	H	-1.750655	0.939097	-0.401025
N	0.660411	-0.726737	-0.000321	H	-0.441167	1.693060	0.740601
O	-0.633468	-0.604995	0.000197	O	-0.745099	-1.077620	0.162394
C	-1.302778	0.509567	-0.000131	N	0.041344	-0.005524	-0.372189
H	-0.797245	1.453962	-0.001158	O	1.329856	0.118333	0.141162
H	-2.365547	0.358752	0.000651	H	1.824528	-0.538126	-0.357423

singlet ts1-6a			
C	1.539495	0.274471	-0.156528
H	2.511666	-0.045923	0.184189
H	1.318154	1.250046	-0.546640
O	0.532118	-0.589811	-0.014682
N	-0.419629	0.212494	0.519385
O	-1.523402	-0.017917	-0.292779
H	-2.199120	0.523425	0.125616

Cartesian coordinates of reactants, complexes, transition states of **Figure S9.**

triplet 4				**triplet 6a**			
O	-1.02707	-0.81102	0.009968	O	1.67268	-0.05434	-0.01559
H	-1.77039	-0.20881	0.139225	H	1.480097	-1.00231	-0.01855
N	0.015116	0.091839	-0.26931	N	0.483301	0.578083	-0.00576
O	-0.15987	1.270735	0.125911	O	-0.45711	-0.45674	0.058947
C	1.278979	-0.50915	0.026934	C	-1.71097	0.094121	-0.08524
H	1.371889	-0.97476	0.997035	H	-1.82689	1.118835	0.229989
H	2.114329	-0.08211	-0.49973	H	-2.49507	-0.63923	-0.0065
triplet 1				**triplet 5b**			
C	0	0.70315	0	C	0.599069	0.580663	0.193352
H	-0.59335	1.008547	0.878415	H	1.001189	1.472422	-0.27188
H	-0.59335	1.008547	-0.87842	H	0.515123	0.716492	1.274305
O	1.172706	1.377651	0	O	-1.52324	-0.43537	0.120741
N	0.195284	-0.73529	0	N	-0.7747	0.423586	-0.32124
O	-1.07743	-1.23994	0	O	1.423802	-0.48581	-0.14842
H	-0.94252	-2.19065	0	H	1.107693	-1.26854	0.307557
triplet CH(OH)NOH				**triplet CH_2NOH….O**			
C	0.62214	0.5988	0.14563	C	-1.90657	-0.371972	-0.000004
H	0.681559	1.10892	1.097251	N	-0.636179	-0.362747	0.000006
H	1.294715	-0.9049	-0.78747	O	-0.145691	0.940083	0.000001
O	1.506898	-0.43037	0.021084	H	-2.385068	-1.339324	-0.000001
N	-0.62773	0.468649	-0.48189	H	-2.492777	0.540683	-0.00001
O	-1.39335	-0.39946	0.278579	H	0.803679	0.798687	-0.000002
H	-2.22339	-0.43873	-0.20767	O	2.641545	-0.343706	-0.000002

Triplet ts 1-CH(OH)NOH			
C	0.6377	0.456443	0.269067
H	1.024985	-0.58309	0.87651
H	1.029728	1.412612	0.605033
O	1.529128	-0.46621	-0.21977
N	-0.63077	0.54313	-0.36389
O	-1.43202	-0.41115	0.191698
H	-2.2424	-0.35126	-0.32416

Triplet ts 1-CH_2NOH….O			
O	1.012776	-1.101448	0.091638
H	0.391127	-1.771957	-0.195650
N	0.366086	0.082924	-0.259086
O	-2.516755	0.047640	0.068193
C	1.065813	1.093314	0.059921
H	2.033995	0.999665	0.539362
H	0.649230	2.062404	-0.168282

Triplet ts 1-NOH + CH_2O			
C	-0.946818	0.47011	0.221846
O	-1.31656	-0.679547	-0.167461
N	0.718251	0.630859	-0.317508
O	1.368869	-0.440463	0.155443
H	-1.341172	1.360815	-0.277618
H	-0.722118	0.610289	1.287785
H	2.297969	-0.247697	-0.02254

Triplet ts 4-5b			
C	-0.59107	1.179026	0.035094
H	-0.08117	1.961536	-0.49719
H	-1.09006	1.344856	0.979276
O	-0.88784	-1.06424	0.092414
N	-0.29049	-0.09068	-0.33401
O	1.502153	-0.12167	0.200124
H	1.836587	-0.25846	-0.69486

Triplet ts 4-CH_2NOH…O			
C	0.364424	1.262683	0.056249
O	-1.486351	-0.337113	0.142029
N	0.074127	0.054443	-0.388993
H	-0.27537	2.061493	-0.275136
H	1.164004	1.405254	0.768068
O	0.949584	-0.879819	0.13448
H	0.700066	-1.688487	-0.319544

Triplet ts 5b-CH(OH)NOH			
C	0.405917	-0.29426	0.397866
H	0.584905	-0.76798	1.359325
H	1.357035	0.722433	-0.8767
O	1.553245	0.007907	-0.262
N	-0.66244	0.657722	0.324261
O	-1.45821	-0.22285	-0.34737
H	-0.50068	-1.07339	-0.26467

Triplet ts 6a-NOH + CH_2O			
C	-1.780718	0.08108	-0.000122
O	-0.616023	-0.4756	0.000121
N	0.631391	0.613865	0.000169
O	1.656366	-0.252474	-0.000053
H	-2.245529	0.361002	-0.941262
H	-2.245888	0.361024	0.940831
H	2.433249	0.319035	-0.000569

Cartesian coordinates of reactant, transition states and products of **Figure S10.**

singlet 1			
C	0.889995	0.603607	-0.064256
H	1.676206	0.977975	0.580008
H	0.649171	1.189807	-0.942470
O	0.796848	-0.781783	-0.208125
N	-0.204439	-0.042106	0.583854
O	-1.331231	0.154604	-0.225854
H	-1.959215	-0.477251	0.132850

I1			
C	-0.834177	-0.821229	-0.342123
H	-1.600130	-1.122098	0.384209
H	-0.414659	1.133538	-0.774722
O	-0.826964	0.822415	0.045148
N	0.168429	-0.246745	0.510936
O	1.316655	-0.035694	-0.237331
H	1.923316	0.349383	0.404169

P2			
C	0.000000	0.762211	0.000000
H	-0.064007	1.320435	0.925278
H	-0.064007	1.320435	-0.925278
O	-0.635379	-0.502804	0.000000
N	0.744435	-0.455958	0.000000

I2			
C	1.428087	0.607116	0.035748
H	-0.865849	-1.109311	0.828761
H	0.575676	1.355247	0.090538
O	1.131623	-0.533131	-0.051141
N	-0.911482	-0.740055	-0.121166
O	-1.187932	0.580436	0.109714
H	-1.447507	0.913314	-0.754205

ts1-I1			
C	0.851186	-0.810319	0.231942
H	1.618338	-1.122104	-0.476826
H	0.928400	0.332140	0.986698
O	0.759736	0.870896	0.006801
N	-0.166730	-0.143104	-0.513143
O	-1.328233	-0.086435	0.246257
H	-1.938766	0.377919	-0.333991

ts1-I2			
C	1.153892	0.671539	0.044877
H	0.274294	0.514295	1.133633
H	0.633388	1.302862	-0.693168
O	0.803366	-0.669506	-0.303403
N	-0.263210	-0.306900	0.527921
O	-1.308044	0.263714	-0.217548
H	-1.951135	-0.451752	-0.237568

P1			
C	0.867166	0.598150	-0.235015
H	1.639430	1.279598	0.106199
O	0.902812	-0.730431	-0.074526
N	-0.214068	0.137194	0.545764
O	-1.329222	0.062005	-0.270622
H	-1.932673	-0.481450	0.244729

Cartesian coordinates of conformers of **1** and transition states in **Figure S14.**

1a				**1a'**			
C	0.889995	0.603607	-0.064256	C	-0.889995	0.603607	-0.064256
H	1.676206	0.977975	0.580008	H	-1.676206	0.977975	0.580008
H	0.649171	1.189807	-0.942470	H	-0.649171	1.189807	-0.942470
O	0.796848	-0.781783	-0.208125	O	-0.796848	-0.781783	-0.208125
N	-0.204439	-0.042106	0.583854	N	0.204439	-0.042106	0.583854
O	-1.331231	0.154604	-0.225854	O	1.331231	0.154604	-0.225854
H	-1.959215	-0.477251	0.132850	H	1.959215	-0.477251	0.132850
1b				**1b'**			
C	0.891092	-0.599108	0.115372	C	-0.891092	-0.599108	0.115372
H	1.719855	-0.980089	-0.467948	H	-1.719855	-0.980089	-0.467948
H	0.645019	-1.137694	1.023435	H	-0.645019	-1.137694	1.023435
O	0.745243	0.799084	0.159670	O	-0.745243	0.799084	0.159670
N	-0.190767	-0.013516	-0.613361	N	0.190767	-0.013516	-0.613361
O	-1.395468	-0.086339	0.094124	O	1.395468	-0.086339	0.094124
H	-1.174254	0.105087	1.015461	H	1.174254	0.105087	1.015461

ts1a-1b				**ts1a'-1b'**			
C	-0.900835	-0.586548	-0.155848	C	0.900835	-0.586548	-0.155848
O	-0.728297	0.806692	-0.126024	H	1.749184	-0.972299	0.394766
N	0.178179	-0.048951	0.624629	H	0.631565	-1.081576	-1.079020
O	1.383531	-0.137726	-0.121098	O	0.728297	0.806692	-0.126024
H	-1.749184	-0.972299	0.394766	N	-0.178179	-0.048951	0.624629
H	-0.631565	-1.081576	-1.079020	O	-1.383531	-0.137726	-0.121098
H	1.296635	0.564087	-0.776089	H	-1.296635	0.564087	-0.776089
ts1a-1b'				**ts1a'-1b**			
C	1.054254	0.588319	0.018231	C	-1.054254	0.588320	0.018231
H	1.524642	0.975222	-0.883997	H	-1.524642	0.975223	-0.883996
H	1.468826	0.964582	0.953072	H	-1.468825	0.964582	0.953072
O	0.819933	-0.863553	0.003978	O	-0.819933	-0.863553	0.003978
N	-0.223391	0.136371	-0.028789	N	0.223391	0.136371	-0.028789
O	-1.555925	0.062853	-0.102326	O	1.555925	0.062853	-0.102326
H	-1.867318	-0.018718	0.809846	H	1.867318	-0.018718	0.809846

Table S11. (Figures 1, 4, S9, S10, S14 energy tables)

Singlet adiabatic B3LYP/cc-pVTZ// CCSD(T)/CBS ionization energies (IE) of CH_3NO_2 isomers depicted in **Figure 1**.

	B3LYP/ cc-pVTZ[a]	E_{zpc} [b]	**CCSD(T)/cc-pVDZ**	**CCSD(T)/cc-pVTZ**	**CCSD(T)/cc-pVQZ**	**CCSD(T)/ CBS**	**IP(eV)**[c]
1a	-245.015030	0.049012	-244.371494	-244.623838	-244.699796	-244.742402	9.99
1a^{+}	-244.658487	0.049065	-244.022911	-244.263733	-244.335335	-244.375396	
2	-245.059777	0.049666	-244.413738	-244.662517	-244.739511	-244.782942	11.10
2^{+}	-244.658031	0.045620	-244.025862	-244.260102	-244.331061	-244.370915	
3a	-245.056860	0.048189	-244.415640	-244.661169	-244.736297	-244.778579	10.50
3a^{+}	-244.679003	0.048150	-244.047622	-244.281954	-244.352805	-244.392584	
3b	-245.056194	0.047871	-244.412242	-244.659105	-244.734403	-244.776754	10.31
3b^{+}	-244.685027	0.047930	-244.052796	-244.287380	-244.358081	-244.397748	
4a	-245.038672	0.049045	-244.384900	-244.638256	-244.715781	-244.759413	9.57
4a^{+}	-244.694883	0.048176	-244.056591	-244.294335	-244.366452	-244.406968	
4b	-245.028956	0.048099	-244.373019	-244.626918	-244.704529	-244.748201	9.56
4b^{+}	-244.683924	0.047477	-244.044561	-244.283345	-244.355573	-244.396129	
5a	-245.057024	0.047988	-244.416740	-244.665376	-244.742061	-244.785289	8.77
5a^{+}	-244.751333	0.047202	-244.119078	-244.350922	-244.422055	-244.462110	
5b	-245.063650	0.048498	-244.422992	-244.671543	-244.748101	-244.791245	8.90
5b^{+}	-244.751523	0.047411	-244.119344	-244.351777	-244.423001	-244.463099	
6a	-244.977334	0.047504	-244.330346	-244.580384	-244.656400	-244.699126	8.18
6a^{+}	-244.686126	0.046991	-244.050207	-244.286622	-244.357912	-244.397914	
6b	-244.968248	0.046017	-244.319742	-244.569864	-244.645841	-244.688537	7.79
6b^{+}	-244.691591	0.046923	-244.055784	-244.292007	-244.363162	-244.403079	
7a	-245.103306	0.049813	-244.452600	-244.706315	-244.784316	-244.828258	9.50
7a^{+}	-244.760273	0.049383	-244.128761	-244.365626	-244.437990	-244.478704	
7b	-245.101492	0.049815	-244.452600	-244.704589	-244.781964	-244.825541	9.65
7b^{+}	-244.753538	0.048327	-244.120217	-244.356559	-244.428745	-244.469357	
8a	-245.098367	0.050154	-244.453032	-244.705878	-244.783262	-244.826816	9.66
8a^{+}	-244.755142	0.050127	-244.121532	-244.359048	-244.431326	-244.471960	

8b	-245.093667	0.049595	-244.446662	-244.699455	-244.776670	-244.820112	9.42
8b$^+$	-244.759451	0.050149	-244.124337	-244.361909	-244.434099	-244.474671	
9a	-245.065029	0.049438	-244.409643	-244.665182	-244.744176	-244.788726	8.38
9a$^+$	-244.767040	0.050439	-244.130344	-244.368390	-244.440859	-244.481603	
9b	-245.064917	0.049909	-244.407645	-244.665197	-244.744987	-244.790005	8.47
9b$^+$	-244.764860	0.050746	-244.128518	-244.366844	-244.439383	-244.480165	
10a	-245.193115	0.051074	-244.545078	-244.799931	-244.878385	-244.922593	10.58
10a$^+$	-244.818175	0.049383	-244.181259	-244.419219	-244.491460	-244.532052	
10b	-245.181771	0.051054	-244.533951	-244.789234	-244.867638	-244.911798	10.74
10b$^+$	-244.798788	0.051110	-244.165817	-244.404199	-244.476462	-244.517054	
11	-245.161752	0.051041	-244.515371	-244.771032	-244.849190	-244.893170	9.94
11$^+$	-244.806940	0.048815	-244.173327	-244.412558	-244.485092	-244.525838	
12	-244.958223	0.050392	-244.316600	-244.569256	-244.644319	-244.686309	9.20
12$^+$	-244.630754	0.049409	-243.992215	-244.236236	-244.307409	-244.347068	
13	-244.991249	0.050197	-244.348821	-244.601980	-244.677497	-244.719776	9.04
13$^+$	-244.668664	0.050293	-244.033121	-244.276314	-244.347846	-244.387776	
14a	-245.093937	0.049447	-244.446876	-244.698545	-244.775006	-244.817976	9.48
14a$^+$	-244.753562	0.047034	-244.117804	-244.354844	-244.426850	-244.467316	
14b	-245.103658	0.050382	-244.458392	-244.709529	-244.785956	-244.828922	9.39
14b$^+$	-244.764737	0.048257	-244.131785	-244.369002	-244.441097	-244.481617	
15	-244.937083	0.047482	-244.295344	-244.545579	-244.619581	-244.660938	10.71
15$^+$	-244.552113	0.045317	-243.917889	-244.157864	-244.226969	-244.265369	

[a] B3LYP/cc-pVTZ energy with zero-point energy correction in hartree.

[b] zero-point energy by B3LYP/cc-pVTZ in hartree.

[c] relative energy by CCSD(T)/CBS with B3LYP/cc-pVTZ zero-point energy correction.

CCSD/cc-pVTZ//MRCI/CBS energies of the CH_3NO_2 isomers (structures in **Figure 1**) on the adiabatic singlet ground state potential energy surface.

	CCSD/ cc-pVTZ + E_{zpc} [a]	E_{zpc} [b]	MCSCF(8,8)/ cc-pVDZ	MCSCF(8,8)/ cc-pVTZ	MCSCF(8,8)/ cc-pVQZ	MRCI/ cc-pVDZ	MRCI/ cc-pVTZ	MRCI/ cc-pVQZ	MRCI/ CBS	E[c] (kJ/mol)
1a	-244.534823	0.050337	-243.785238	-243.862798	-243.881616	-244.360918	-244.600271	-244.672145	-244.712441	96
1b	-244.528428	0.049677	-243.778046	-243.855889	-243.874290	-244.353671	-244.593205	-244.666163	-244.707186	108
2	-244.570194	0.050701	-243.803629	-243.887336	-243.906971	-244.402571	-244.635515	-244.708239	-244.749332	0
3a	-244.571212	0.049463	-243.831785	-243.906309	-243.924997	-244.406463	-244.638760	-244.709727	-244.749655	-4
3b	-244.570088	0.048840	-243.831305	-243.907327	-243.926296	-244.403337	-244.637104	-244.708266	-244.748274	-2
4a	-244.547014	0.050174	-243.774400	-243.852207	-243.871608	-244.374400	-244.613934	-244.687011	-244.728113	54
4b	-244.535735	0.049369	-243.772013	-243.836820	-243.856768	-244.363929	-244.602207	-244.675384	-244.716599	82
5a	-244.579772	0.049372	-243.841420	-243.917215	-243.936768	-244.408266	-244.644181	-244.716667	-244.757497	-25
5b	-244.584601	0.049810	-243.841704	-243.917285	-243.936867	-244.413046	-244.648694	-244.721055	-244.761810	-35
6a	-244.483961	0.048434	-243.722781	-243.799339	-243.818429	-244.247742	-244.460068	-244.524675	-244.560995	214
6b	-244.474650	0.047035	-243.711527	-243.788954	-243.808247	-244.236096	-244.448502	-244.512993	-244.549231	241
7a	-244.618869	0.051068	-243.866450	-243.931935	-243.951891	-244.442810	-244.680561	-244.754065	-244.795520	-120
7b	-244.618157	0.051055	-243.871658	-243.942112	-243.961604	-244.443465	-244.681625	-244.754700	-244.795850	-121
8a	-244.617846	0.051306	-243.850195	-243.925712	-243.944807	-244.442816	-244.681514	-244.754478	-244.795533	-120
8b	-244.612574	0.050635	-243.845492	-243.921357	-243.940364	-244.436689	-244.675366	-244.748164	-244.789109	-105
9a	-244.575298	0.050563	-243.807166	-243.886074	-243.891373	-244.400519	-244.642151	-244.713432	-244.753246	-11
9b	-244.574649	0.051015	-243.804154	-243.885322	-243.906554	-244.397527	-244.641688	-244.717082	-244.759592	-26
10a	-244.713279	0.052441	-243.962357	-244.041311	-244.061186	-244.534741	-244.776801	-244.851209	-244.893124	-373
10b	-244.702456	0.052332	-243.947538	-244.026141	-244.046044	-244.524712	-244.766793	-244.840938	-244.882675	-346
11	-244.684150	0.052240	-243.930647	-244.009834	-244.029737	-244.440683	-244.659555	-244.726695	-244.861767	-291
12	-244.478600	0.051585	-243.742591	-243.820075	-243.840521	-244.307581	-244.547714	-244.618985	-244.658845	227
13	-244.513491	0.051626	-243.769525	-243.848068	-243.866273	-244.338868	-244.580775	-244.652174	-244.692060	143
14a	-244.611285	0.050753	-243.849080	-243.938174	-243.957238	-244.366001	-244.584619	-244.649875	-244.789288	-105
14b	-244.621125	0.051521	-243.865238	-243.947605	-243.955090	-244.378742	-244.593764	-244.656578	-244.797829	-125
15	-244.455655	0.048469	-243.733080	-243.809614	-243.827374	-244.223779	-244.438305	-244.501519	-244.635073	294

[a] CCSD/cc-pVTZ energy with zero-point energy correction in hartree.

[b] zero-point energy by CCSD/cc-pVTZ in hartree.

[c] relative energy by MRCI/CBS with CCSD/cc-pVTZ zero-point energy correction.

CCSD/cc-pVTZ//CCSD(T)/CBS energies on the adiabatic singlet and triplet ground state potential energy surfaces, of all the reactants, products and transition states depicted in **Figure 4** along with CPMCSCF/TZVPP//CCSD(T)/CBS energies of minimum-energy crossing points (MSX) structures shown in **Figure 4**.

	CCSD /cc-pVTZ + E_{zpc}[a]	E_{zpc} [b]	CCSD(T)/ cc-pVDZ	CCSD(T)/ cc-pVTZ	CCSD(T)/ cc-pVQZ	CCSD(T)/ CBS	E(kJ/mol)[c]
CH_2 (a^{1}A$_1$)+HONO (X^{1}A)	-244.420205	0.037595	-244.249423	-244.494599	-244.569458	-244.611571	37
CH_2 (X^{3}B$_1$)+HONO (X^{1}A)	-244.437425	0.038275	-244.268627	-244.511068	-244.584878	-244.626376	0.0
1 (C$_s$, ^{3}A')	-244.504471	0.047093	-244.335858	-244.582129	-244.657183	-244.699390	-169
4 (C$_1$, ^{3}A)	-244.475196	0.046299	-244.306597	-244.555776	-244.632107	-244.675077	-107
6a (C$_1$, ^{3}A)	-244.474187	0.045524	-244.305905	-244.553256	-244.628191	-244.670280	-96
ts4 (C$_1$, ^{3}A)	-244.423508	0.040672	-244.258726	-244.501304	-244.575469	-244.617201	30
ts6a (C$_1$, ^{3}A)	-244.413358	0.040652	-244.249054	-244.491361	-244.565537	-244.607287	56
ts4-6a (C$_1$, ^{3}A)	-244.374740	0.043295	-244.207746	-244.458558	-244.534051	-244.576396	144
1-MSX[d]		0.051147	-244.336073	-244.583682	-244.658890	-244.701154	-162
4-MSX[d]		0.048862	-244.299105	-244.548461	-244.624713	-244.667622	-80
6a-MSX[d]		0.048063	-244.302303	-244.550287	-244.625431	-244.667639	-83
1 (C$_1$, ^{1}A)	-244.534823	0.050337	-244.370826	-244.623586	-244.699706	-244.742407	-273
4 (C$_s$, ^{1}A')	-244.547014	0.050174	-244.384437	-244.638137	-244.715809	-244.759529	-318
6a (C$_1$, ^{1}A)	-244.483961	0.048434	-244.330107	-244.580361	-244.656475	-244.699259	-165
ts1-4 (C$_1$, ^{1}A)	-244.443859	0.046960	-244.278019	-244.533374	-244.611601	-244.655639	-54
ts1-6a (C$_1$, ^{1}A)	-244.460315	0.046698	-244.310816	-244.560315	-244.635760	-244.678119	-114

CCSD/cc-pVTZ//MRCI/CBS energies on the adiabatic singlet and triplet ground state potential energy surfaces, of all the reactants, products and transition states depicted in **Figure 4** along with CPMCSCF/TZVPP//MRCI/CBS energies of minimum-energy crossing points (MSX) structures shown in **Figure 4**.

	CCSD/ cc-pVTZ + E_{zpc} [a]	E_{zpc} [b]	MCSCF(8,8)/ cc-pVDZ	MCSCF(8,8)/ cc-pVTZ	MCSCF(8,8)/ cc-pVQZ	MRCI/ cc-pVDZ	MRCI/ cc-pVTZ	MRCI/ cc-pVQZ	MRCI/ CBS	E[e] (kJ/mol)
$CH_2(a^1A_1)$+HONO(X^1A)	-244.437425	0.038275	-243.6836447	-243.7587897	-243.77778	-244.1870922	-244.3933093	-244.4562052	-244.4915801	0
$CH_2(X^3B_1)$+HONO(X^1A)	-244.420205	0.037595	-243.6645694	-243.7417896	-243.7612301	-244.1683539	-244.3771584	-244.4409628	-244.4768624	35
1 (C_s, $^3A'$)	-244.504471	0.047093	-243.734595	-243.817704	-243.836502	-244.250704	-244.464348	-244.528026	-244.563671	-171
4 (C_1, ^3A)	-244.475196	0.046299	-243.689095	-243.764519	-243.783376	-244.218637	-244.429609	-244.494183	-244.530528	-100
6a (C_1, ^3A)	-244.474187	0.045524	-243.708141	-243.782962	-243.801725	-244.223971	-244.433790	-244.497470	-244.533250	-101
ts4 (C_1, ^3A)	-244.423508	0.040672	-243.656527	-243.729229	-243.747484	-244.169843	-244.374564	-244.437135	-244.472342	45
ts6a (C_1, ^3A)	-244.413358	0.040652	-243.663232	-243.736081	-243.754496	-244.167653	-244.373015	-244.435903	-244.471302	54
ts4-6a (C_1, ^3A)	-244.374740	0.043295	-243.599313	-243.676663	-243.695457	-244.119888	-244.332170	-244.396023	-244.431834	151
1-MSX[d]		0.051147	-243.744844	-243.818775	-243.837500	-244.251301	-244.461395	-244.525242	-244.561125	-151
4-MSX[d]		0.048862	-243.706456	-243.783223	-243.802418	-244.219465	-244.432200	-244.497195	-244.533763	-86
6a-MSX[d]		0.048063	-243.717685	-243.793613	-243.812502	-244.223099	-244.434345	-244.498461	-244.534485	-86
1 (C_1, ^1A)	-244.534823	0.050337	-243.7852376	-243.8627984	-243.8816156	-244.2936165	-244.5094119	-244.5743787	-244.6108211	-282
4 (C_s, $^1A'$)	-244.547014	0.050174	-243.7743999	-243.852207	-243.8716083	-244.302377	-244.517969	-244.583865	-244.620943	-324
6a (C_1, ^1A)	-244.483961	0.048434	-243.722781	-243.799339	-243.818429	-244.247742	-244.460068	-244.524675	-244.560995	-173
ts1-4 (C_1, ^1A)	-244.443859	0.046960	-243.680617	-243.762085	-243.782733	-244.196747	-244.414723	-244.481450	-244.519008	-59
ts1-6a (C_1, ^1A)	-244.460315	0.046698	-243.709547	-243.786049	-243.804943	-244.229125	-244.441053	-244.505112	-244.541076	-122

[a] CCSD/cc-pVTZ energy with zero-point energy correction in hartree.

[b] zero-point energy by CCSD/cc-pVTZ in hartree.

[c] relative energy by CCSD(T)/CBS with CCSD/cc-pVTZ zero-point energy correction.

[d] geometry optimized by CPMCSCF/TZVPP.

[e] relative energy by MRCI/CBS with CCSD/cc-pVTZ zero-point energy correction.

CCSD/cc-pVTZ//CCSD(T)/CBS energies on the adiabatic triplet ground state potential energy surface, of all the reactants, products and transition states, illustrated in **Figure S9.**

	CCSD / cc-pVTZ + E_{zpc}[a]	E_{zpc} [b]	CCSD(T)/ cc-pVDZ	CCSD(T)/ cc-pVTZ	CCSD(T)/ cc-pVQZ	CCSD(T)/ CBS	E(kJ/mol)[c]
4 (C_1, ^3A)	-244.475196	0.046299	-244.306597	-244.555776	-244.632107	-244.675077	0
6a (C_1, ^3A)	-244.474187	0.045524	-244.305905	-244.553256	-244.628191	-244.670280	11
1 (C_s, $^3A'$)	-244.504471	0.047093	-244.335858	-244.582129	-244.657183	-244.699390	-62
5b (C_1, ^3A)	-244.551009	0.049854	-244.386829	-244.6343914	-244.7103874	-244.7531863	-196
CH(OH)NOH **(C_1, ^3A)**	-244.514055	0.048044	-244.344688	-244.594919	-244.671307	-244.714279	-98
CH_2NOH-O (C_1, ^3A)	-244.463806	0.046034	-244.3027293	-244.5402374	-244.6122099	-244.6526365	58
NOH (C_s, $^3A''$)+ CH_2O(C_{2v}, $^1A_1$)	-244.521494	0.041185	-244.352393	-244.593661	-244.667192	-244.708542	-111
ts1- CH(OH)NOH **(C_1,^3A)**	-244.450822	0.043024	-244.278702	-244.528733	-244.6047828	-244.647591	64
ts1-CH_2NOH-O (C_1,^3A)	-244.461103	0.046126	-244.299813	-244.538397	-244.610685	-244.651288	62
ts1-(^{3}NOH+$^1CH_2O$) (C_1,^3A)	-244.485895	0.045042	-244.319740	-244.565172	-244.639917	-244.681944	-21
ts4-5b (C_1,^3A)	-244.456756	0.042897	-244.289900	-244.536365	-244.612498	-244.655427	-64
ts4-CH_2NOH-O (C_1,^3A)	-244.434055	0.044920	-244.269211	-244.5137523	-244.5883417	-244.630294	114
ts5b- CH(OH)NOH **(C_1,^3A)**	-244.469312	0.043343	-244.301972	-244.550091	-244.625585	-244.668024	11
ts6a-(^{3}NOH+$^1CH_2O$) (C_1,^3A)	-244.459467	0.042691	-244.292215	-244.537334	-244.611818	-244.653678	47

CCSD/cc-pVTZ//MRCI/CBS energies on the adiabatic triplet ground state potential energy surface, of all the reactants, products and transition states depicted in **Figure S9.**

	CCSD/ cc-pVTZ + E_{zpc} [a]	E_{zpc} [b]	MCSCF(8,8)/ cc-pVDZ	MCSCF(8,8)/ cc-pVTZ	MCSCF(8,8)/ cc-pVQZ	MRCI/ cc-pVDZ	MRCI/ cc-pVTZ	MRCI/ cc-pVQZ	MRCI/ CBS	E^d (kJ/mol)
4 (C_1, ^3A)	-244.475196	0.046299	-243.689095	-243.764519	-243.783376	-244.218637	-244.429609	-244.494183	-244.530528	0
6a (C_1, ^3A)	-244.474187	0.045524	-243.708141	-243.782962	-243.801725	-244.223971	-244.433790	-244.497470	-244.533250	-1
1 (C_s, $^3A'$)	-244.504471	0.047093	-243.734595	-243.817704	-243.836502	-244.250704	-244.464348	-244.528026	-244.563671	-71
5b (C_1, ^3A)	-244.551009	0.049854	-243.751721	-243.827188	-243.846429	-244.294660	-244.503443	-244.567677	-244.603868	-196
CH(OH)NOH**(C_1, ^3A)**	-244.514055	0.048044	-243.740163	-243.816235	-243.835622	-244.261677	-244.473716	-244.539071	-244.575907	-103
CH_2NOH-O(C_1, ^3A)	-244.463806	0.046034	-243.729073	-243.798633	-243.816916	-244.227043	-244.428643	-244.489961	-244.524429	41
NOH(C_s,$^3A''$)+ CH_2O (C_{2v}, $^1A_1$)	-244.521494	0.041185	-243.780373	-243.853184	-243.872021	-244.277465	-244.482447	-244.545022	-244.580222	-121
ts1-CH(OH)NOH **(C_1,^3A)**	-244.450822	0.043024	-243.667928	-243.742239	-243.761011	-244.192596	-244.403082	-244.467136	-244.503145	61
ts1-CH2NOH-O (C_1,^3A)	-244.461103	0.046126	-243.749086	-243.818008	-243.8153182	-244.230857	-244.433174	-244.487990	-244.518033	50
ts1-(^{3}NOH+$^1CH_2O$) (C_1,^3A)	-244.485895	0.045042	-243.727141	-243.801072	-243.819809	-244.237532	-244.445326	-244.508622	-244.544213	-28
ts4-5b (C_1,^3A)	-244.456756	0.042897	-243.675828	-243.747775	-243.766535	-244.200447	-244.407460	-244.471088	-244.506930	46
ts4-CH_2NOH-O (C_1,^3A)	-244.434055	0.044920	-243.668701	-243.741182	-243.759691	-244.187209	-244.393768	-244.456614	-244.491942	103
ts5b-CH(OH)NOH **(C_1,^3A)**	-244.469312	0.043343	-243.698747	-243.773136	-243.792001	-244.217848	-244.428104	-244.492262	-244.528351	5
ts6a-(^{3}NOH+$^1CH_2O$) (C_1,^3A)	-244.459467	0.042691	-243.690812	-243.778355	-243.767339	-244.209448	-244.419810	-244.473773	-244.502958	45

[a] CCSD/cc-pVTZ energy with zero-point energy correction in hartree.

[b] zero-point energy by CCSD/cc-pVTZ in hartree.

[c] relative energy by CCSD(T)/CBS with CCSD/cc-pVTZ zero-point energy correction.

[d] relative energy by MRCI/CBS with CCSD/cc-pVTZ zero-point energy correction.

CCSD/cc-pVTZ//CCSD(T)/CBS energies on the adiabatic singlet ground state potential energy surface, of all the reactants, products and transition states shown in **Figure S10**.

	CCSD / cc-pVTZ + E_{zpc}[a]	E_{zpc}[b]	CCSD(T)/ cc-pVDZ	CCSD(T)/ cc-pVTZ	CCSD(T)/ cc-pVQZ	CCSD(T)/ CBS	E(kJ/mol)[c]
1 (C_1, ^1A)	-244.534823	0.050337	-244.370826	-244.623586	-244.699706	-244.742407	0
I1 (C_1, ^1A)	-244.432415	0.048383	-244.269008	-244.520782	-244.596343	-244.638702	267
I2 (C_1, ^1A)	-244.474634	0.046559	-244.331929	-244.576462	-244.651977	-244.694557	116
ts1-I1 (C_1, A)	-244.420224	0.04419	-244.248507	-244.499638	-244.575137	-244.617475	292
ts1-I2 (C_1, A)	-244.404712	0.043958	-244.238921	-244.490302	-244.565824	-244.608169	336
P2 (C_s, $^2A''$) + OH	-244.460501	0.041484	-244.288237	-244.533708	-244.607452	-244.648799	223
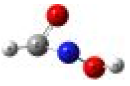 **(C_1, ^2A) + H**	-244.375706	0.03702	-244.203678	-244.449752	-244.524598	-244.566671	427

CCSD/cc-pVTZ//MRCI/CBS energies on the adiabatic singlet ground state potential energy surface, of all the reactants, products and transition states shown in **Figure S10**.

	CCSD/ cc-pVTZ + E_{zpc}[a]	E_{zpc}[b]	MCSCF(8,8)/ cc-pVDZ	MCSCF(8,8)/ cc-pVTZ	MCSCF(8,8)/ cc-pVQZ	MRCI/ cc-pVDZ	MRCI/ cc-pVTZ	MRCI/ cc-pVQZ	MRCI/ CBS	E[d] (kJ/mol)
1 (C_1, ^1A)	-244.534823	0.050337	-243.785238	-243.862798	-243.881616	-244.293616	-244.509412	-244.574379	-244.712441	0
I1 (C_1, ^1A)	-244.432415	0.048383	-243.655909	-243.732689	-243.751351	-244.183202	-244.396195	-244.460259	-244.604531	278
I2 (C_1, ^1A)	-244.474634	0.046559	-243.727256	-243.798045	-243.816431	-244.250359	-244.455965	-244.519697	-244.664665	115
ts1-I1 (C_1, A)	-244.420224	0.04419	-243.657375	-243.732713	-243.751143	-244.172803	-244.385524	-244.449648	-244.591978	300
ts1-I2 (C_1, A)	-244.404712	0.043958	-243.628165	-243.688749	-243.707287	-244.152314	-244.359782	-244.423636	-244.570769	355
P2 (C_s, $^2A''$) + OH	-244.460501	0.041484	-243.706104	-243.779710	-243.798395	-244.209245	-244.417198	-244.479701	-244.618303	224
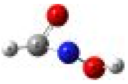 **(C_1, ^2A) + H**	-244.375706	0.03702	-243.606915	-243.681784	-243.700253	-244.120570	-244.329405	-244.393004	-244.533158	436

[a] CCSD/cc-pVTZ energy with zero-point energy correction in hartree.

[b] zero-point energy by CCSD/cc-pVTZ in hartree.

[c] relative energy by CCSD(T)/CBS with CCSD/cc-pVTZ zero-point energy correction.

[d] relative energy by MRCI/CBS with CCSD/cc-pVTZ zero-point energy correction.

CCSD/cc-pVTZ//CCSD(T)/CBS energies on the adiabatic singlet ground state potential energy surface, of all the conformers of **1** shown in **Figure S14**.

	CCSD/ cc-pVTZ + E_{zpc} [a]	E_{zpc} [b]	CCSD(T)/ cc-pVDZ	CCSD(T)/ cc-pVTZ	CCSD(T)/ cc-pVQZ	CCSD(T)/ CBS	E^c (kJ/mol)
1a	-244.534823	0.050337	-244.3708256	-244.623586	-244.6997056	-244.7424069	0
1a'	-244.534823	0.050337	-244.3708256	-244.623586	-244.6997056	-244.7424069	0
1b	-244.528428	0.049677	-244.3636847	-244.6165918	-244.6925859	-244.7351972	17
1b'	-244.528428	0.049677	-244.3636847	-244.6165918	-244.6925859	-244.7351972	17
ts1a1b	-244.528509	0.049166	-244.3635023	-244.6161161	-244.6920226	-244.7345848	18
ts1a'1b'	-244.528509	0.049166	-244.3635023	-244.6161161	-244.6920226	-244.7345848	18
ts1a1b'	-244.432741	0.049174	-244.2645138	-244.5193466	-244.5964529	-244.6397497	267
ts1a'1b	-244.432741	0.049174	-244.2645138	-244.5193466	-244.5964529	-244.6397497	267

CCSD/cc-pVTZ//MRCI/CBS energies on the adiabatic singlet ground state potential energy surface, of all the conformers of **1** shown in **Figure S14**.

	CCSD/ cc-pVTZ + E_{zpc} [a]	E_{zpc} [b]	MCSCF(8,8)/ cc-pVDZ	MCSCF(8,8)/ cc-pVTZ	MCSCF(8,8)/ cc-pVQZ	MRCI/ cc-pVDZ	MRCI/ cc-pVTZ	MRCI/ cc-pVQZ	MRCI/ CBS	E^d (kJ/mol)
1a	-244.534823	0.050337	-243.785238	-243.862798	-243.881616	-244.360918	-244.600271	-244.672145	-244.712441	0
1a'	-244.534823	0.050337	-243.785238	-243.862798	-243.881616	-244.360918	-244.600271	-244.672145	-244.712441	0
1b	-244.528428	0.049677	-243.778046	-243.855889	-243.874290	-244.353671	-244.593205	-244.666163	-244.707186	12
1b'	-244.528428	0.049677	-243.778046	-243.855889	-243.874290	-244.353671	-244.593205	-244.666163	-244.707186	12
ts1a1b	-244.528509	0.049166	-243.781420	-243.856855	-243.875215	-244.355482	-244.594325	-244.665816	-244.705870	14
ts1a'1b'	-244.528509	0.049166	-243.781420	-243.856855	-243.875215	-244.355482	-244.594325	-244.665816	-244.705870	14
ts1a1b'	-244.432741	0.049174	-243.675986	-243.755593	-243.774992	-244.254351	-244.495783	-244.568623	-244.609499	267
ts1a'1b	-244.432741	0.049174	-243.675986	-243.755593	-243.774992	-244.254351	-244.495783	-244.568623	-244.609499	267

[a] CCSD/cc-pVTZ energy with zero-point energy correction in hartree.

[b] zero-point energy by CCSD/cc-pVTZ in hartree.

[c] relative energy by CCSD(T)/CBS with CCSD/cc-pVTZ zero-point energy correction.

[d] relative energy by MRCI/CBS with CCSD/cc-pVTZ zero-point energy correction.

References

(1) Jones, B. M.; Kaiser, R. I. Application of Reflectron Time-of-Flight Mass Spectroscopy in the Analysis of Astrophysically Relevant Ices Exposed to Ionization Radiation: Methane (CH4) and D4-Methane (CD4) as a Case Study. *J. Phys. Chem. Lett.* **2013**, *4*, 1965-1971.

(2) Maity, S.; Kaiser, R. I.; Jones, B. M. Formation of complex organic molecules in methanol and methanol–carbon monoxide ices exposed to ionizing radiation – a combined FTIR and reflectron time-of-flight mass spectrometry study. *Phys. Chem. Chem. Phys.* **2015**, *17*, 3081-3114.

(3) Gerakines, P. A.; Hudson, R. L. Infrared Spectra and Optical Constants of Elusive Amorphous Methane. *ApJ* **2015,** *805*, L20.

(4) Fulvio, D.; Sivaraman, B.; Baratta, G. A.; Palumbo, M. E.; Mason, N. J. Novel Measurements of Refractive Index, Density and Mid-Infrared Integrated Band Strengths for Solid O_2, N_2O and NO_2:N_2O_4 Mixtures. *Spectrochim. Acta A* **2009,** *72*, 1007-1013.

(5) Drouin, D.; Couture, A. R.; Joly, D.; Tastet, X.; Aimez, V.; Gauvin, R. CASINO V2.42—A Fast and Easy-to-use Modeling Tool for Scanning Electron Microscopy and Microanalysis Users. *Scanning* **2007**, *29*, 92-101.

(6) Purvis, G. D.; Bartlett, R. J. A Full Coupled-Cluster Singles and Doubles Model: The Inclusion of Disconnected Triples. *J. Chem. Phys.* **1982**, *76*, 1910-1918.

(7) Knowles, P. J.; Hampel, C.; Werner, H. J. Coupled Cluster Theory for High Spin, Open Shell Reference Wave Functions. *J. Chem. Phys.* **1993**, *99*, 5219-5227.

(8) Peterson, K. A.; Woon, D. E.; Jr., T. H. D. Benchmark Calculations with Correlated Molecular Wave Functions. IV. The Classical Barrier Height of the $H+H_2\rightarrow H_2+H$ Reaction. *J. Chem. Phys.* **1994**, *100*, 7410-7415.

(9) Peterson, K. A.; Dunning, T. H. Intrinsic Errors in Several Ab Initio Methods: The Dissociation Energy of N_2. *J. Phys. Chem.* **1995**, *99*, 3898-3901.

(10) Werner, H.-J.; Knowles, P. J.; Knizia, G.; Manby, F. R.; Schütz, M.; Celani, P.; W. Györffy, W.; Kats, D.; Korona, T.; Lindh, R.; Mitrushenkov, A.; Rauhut, G.; Shamasundar, K. R.; Adler, T. B.; Amos, R. D.; Bennie, S. J.; Bernhardsson, A.; Berning, A.; Cooper, D. L.; Deegan, M. J. O.; Dobbyn, A. J.; Eckert, F.; Goll, E.; Hampel, C.; Hesselmann, A.; Hetzer, G.; Hrenar, T.; Jansen, G.; Köppl, C.; Lee, S. J. R.; Liu, Y.; Lloyd, A. W.; Ma, Q.; Mata, R. A.; May, A. J.; McNicholas, S. J.; Meyer, W.; Miller III, T. F.; Mura, M. E.; Nicklass, A.; O'Neill, D. P.; Palmieri, P.; Peng, D.; Pflüger, K.; Pitzer, R.; Reiher, M.; Shiozaki, T.; Stoll, H.; Stone, A. J.; Tarroni, R.; Thorsteinsson, T.; Wang, M.; and Welborn, M. Molpro: A General-Purpose Quantum Chemistry Program Package. *WIREs Comput. Mol. Sci.* **2012,** *2*, 242--253.

(11) Frisch, M. J. T., G. W.; Schlegel, H. B.; Scuseria, G. E.; Robb, M. A.; Cheeseman, J. R.; Scalmani, G.; Barone, V.; Petersson, G. A.; Nakatsuji, H.; Li, X.; Caricato, M.; Marenich, A. V.; Bloino, J.; Janesko, B. G.; Gomperts, R.; Mennucci, B.; Hratchian, H. P.; Ortiz, J. V.; Izmaylov, A. F.; Sonnenberg, J. L.; Williams-Young, D.; Ding, F.; Lipparini, F.; Egidi, F.; Goings, J.; Peng, B.; Petrone, A.; Henderson, T.; Ranasinghe, D.; Zakrzewski, V. G.; Gao, J.; Rega, N.; Zheng, G.; Liang, W.; Hada, M.; Ehara, M.; Toyota, K.; Fukuda, R.; Hasegawa, J.; Ishida, M.; Nakajima, T.; Honda, Y.; Kitao, O.; Nakai, H.; Vreven, T.; Throssell, K.; Montgomery, J. A., Jr.; Peralta, J. E.; Ogliaro, F.; Bearpark, M. J.; Heyd, J. J.; Brothers, E. N.; Kudin, K. N.; Staroverov, V. N.; Keith, T. A.; Kobayashi, R.; Normand, J.; Raghavachari, K.; Rendell, A. P.; Burant, J. C.; Iyengar, S. S.; Tomasi, J.; Cossi, M.; Millam, J. M.; Klene, M.; Adamo, C.; Cammi, R.; Ochterski, J. W.; Martin, R. L.; Morokuma, K.; Farkas, O.; Foresman, J. B.; Fox, D. J., *Gaussian 16, Revision C.01, Gaussian Inc., Wallingford CT, 2016*.

(12) Bennett, C. J.; Brotton, S. J.; Jones, B. M.; Misra, A. K.; Sharma, S. K.; Kaiser, R. I. High-Sensitivity Raman Spectrometer To Study Pristine and Irradiated Interstellar Ice Analogs. *Anal. Chem.* **2013**, *85*, 5659-5665.

(13) Kaiser, R. I.; Maity, S.; Jones, B. M. Infrared and Reflectron Time-of-Flight Mass Spectroscopic Analysis of Methane (CH_4)–Carbon Monoxide (CO) Ices Exposed to Ionization Radiation – Toward the Formation of Carbonyl-Bearing Molecules in Extraterrestrial Ices. *Phys. Chem. Chem. Phys.* **2014**, *16*, 3399-3424.

(14) Kagann, R. H.; Maki, A. G. Infrared Absorption Intensities of Nitrous Acid (HONO) Fundamental Bands. *J. Quant. Spectrosc. Radiat. Transfer* **1983**, *30*, 37-44.

(15) Ulenikov, O. N.; Bekhtereva, E. S.; Albert, S.; Bauerecker, S.; Niederer, H. M.; Quack, M. Survey of the high resolution infrared spectrum of methane ($^{12}CH_4$ and $^{13}CH_4$): Partial Vibrational Assignment Extended Towards 12 000 cm^{-1}. *J. Chem. Phys.* **2014**, *141*, 234302.

(16) He, J.; Gao, K.; Vidali, G.; Bennett, C. J.; Kaiser, R. I. Formation of Molecular Hydrogen From Methane Ice. *ApJ* **2010**, *721*, 1656-1662.